arXiv:0804.0811v1 [astro-ph] 4 Apr 2008

The Early-time Optical Properties of Gamma-Ray Burst Afterglows

A. Melandri[1], C.G. Mundell[1], S. Kobayashi[1], C. Guidorzi[2,3,1], A. Gomboc[4], I.A. Steele[1], R.J. Smith[1], D. Bersier[1], C.J. Mottram[1], D. Carter[1], M.F. Bode[1], P.T. O'Brien[5], N.R. Tanvir[5], E. Rol[5], R. Chapman[6]

axm@astro.livjm.ac.uk

ABSTRACT

We present a multiwavelength analysis of 63 Gamma-Ray Bursts observed with the world's three largest robotic optical telescopes, the Liverpool and Faulkes Telescopes (North and South). Optical emission was detected for 24 GRBs with brightnesses ranging from $R = 10$ to 22 mag in the first 10 minutes after the burst. By comparing optical and X-ray light curves from t = 100 to $\sim 10^6$ seconds, we introduce four main classes, defined by the presence or absence of temporal breaks at optical and/or X-ray wavelengths. While 15/24 GRBs can be modelled with the forward-shock model, explanation of the remaining nine is very challenging in the standard framework even with the introduction of energy injection or an ambient density gradient. Early X-ray afterglows, even segments of light curves described by a power-law, may be due to additional emission from the central engine. 39 GRBs in our sample were not detected and have deep upper limits ($R < 22$ mag) at early time. Of these, only ten were identified by other facilities, primarily at near infrared wavelengths, resulting in a dark burst fraction of $\sim$50%. Additional emission in the early time X-ray afterglow due to late-time central engine activity may also explain some dark bursts by making the bursts brighter than expected in the X-ray band compared to the optical band.

[1]Astrophysics Research Institute, Liverpool John Moores University, Twelve Quays House, Egerton Wharf, Birkenhead, CH41 1LD, UK

[2]Università di Milano Bicocca, Dipartimento di Fisica, piazza della Scienze 3, I-20126 Milano, Italy

[3]INAF Osservatorio Astronomico di Brera, via Bianchi 46, 23807 Merate (LC), Italy

[4]FMF, University of Ljubljana, Jadranska 19, 1000 Ljubljana, Slovenia

[5]Department of Physics and Astronomy, University of Leicester, University Road, Leicester LE1 7RH, UK

[6]Centre for Astrophysics Research, University of Hertfordshire, College Lane, Hatfield AL10 9AB, UK

Subject headings: Gamma rays: bursts

1. Introduction

Gamma Ray Bursts (GRBs) are brief, intense flashes of high energy gamma rays originating at cosmological distances and often associated with subsequent radiation emitted at longer wavelengths from X-ray to radio waves on times scales of minutes to days after the initial gamma ray burst. In the standard model a typical long duration GRB is thought to be formed by the explosion of a compact source that generates an expanding relativistic fireball (Rees & Mészáros 1992). If the central engine remains active for some time several expanding shells with different speeds (different Lorentz factors, Γ) can be produced. The collisions between these shells power the γ-ray prompt emission itself (internal shocks), while the interactions of the relativistic flow with the surrounding medium (external forward shocks) generate the so-called afterglow emission that dominates at longer wavelengths and is more long-lived than the prompt emission (Mészáros 2002, Piran 1999). Assuming that the shock-accelerated electrons producing the radiation have a power-law spectral energy distribution, the afterglow synchrotron emission is expected to exhibit a standard form of spectrum, with two characteristic break frequencies: the typical synchrotron frequency $\nu_{\rm m}$ and the cooling frequency $\nu_{\rm c}$ (Sari, Piran & Narayan 1998). When the forward shock is formed, a reverse shock that propagates backwards into the ejecta is also generated. The brightness of the reverse shock emission decays very rapidly compared to the decay of the forward component. It is predicted that at early time the reverse shock can produce extremely bright optical flashes while at late time the optical flux is completely dominated by the forward shock emission (Mészáros & Rees 1997, Sari & Piran 1999). In reality, the resultant light curve is a complex, time-dependent mixture of these components and unravelling them provides important insight into the physics and energetics of the explosion.

The study of pre-*Swift* bursts allowed the understanding of late time multiband properties of the afterglows confirming many predictions of the fireball model. Well-sampled pre-*Swift* optical light curves were mostly obtained at late times, typically after few hours from the burst event, and exhibited relatively smooth light curves with simple power law decays, showing breaks at late time (hints of a jet evolution) and making clear a strong connection with supernova emission and, thus, the death of massive stars (e.g. Woosley & Bloom 2006, Malesani et al. 2004, Stanek et al. 2003). The advent of the *Swift* satellite (Gehrels et al. 2004) has opened up a new observational window at early times, revealing more complex light curve behaviour than previously known. It is now accepted that the X-ray temporal decay of GRBs observed by *Swift* is well described by a canonical light curve

(Nousek et al. 2006; Zhang et al. 2006); combining the γ-ray (Burst Alert Telescope, BAT, Barthelmy et al. 2005) and X-ray (X-Ray Telescope, XRT, Burrows et al. 2005) data the initial X-ray emission (rapid fall-off for the first hundred seconds) is consistent with the tail of the γ-ray emission (Tagliaferri et al. 2005, O'Brien et al. 2006) and can be modelled by two components that have exactly the same functional form (Willingale et al. 2007). These functions are completely empirical and do not do not provide a physical explanation for the X-ray flares seen in many bursts, but the majority of *Swift* bursts seem to follow this behaviour.

It was clear that rapid response to obtain early-time optical observations with ground based robotic telescopes was required to pin down the open issue of the emission mechanism for the GRB itself and its afterglow. However, the small number of prompt optical observations simultaneous to the GRB γ-ray emission do not yet allow a firm conclusion to be drawn about the GRB emission models (Yost et al. 2007). The statistics of these events remain small due to the fact that the GRBs detected by *Swift* satellite are fainter and located at higher redshift ($< z >= 2.7$, Le & Dermer 2007, Jakobsson et al. 2006) than those detected by previous missions. Large 2-m robotic telescopes, such as the Liverpool and Faulkes (North and South) Telescopes, responding within 1-3 minutes of the burst offer a unique tool for probing early-time light curves over a wide range of brightnesses, allowing the extension of the analysis of GRB properties to unprecedented depth and time coverage.

Based on the theoretical predictions of the forward and reverse shock emission theories, optical light curves at early times should show different shapes depending on the relative contribution of the two components (Kobayashi & Zhang 2003, Zhang, Kobayashi & Mészáros 2003); possible light curve shapes are illustrated in Figure 1. In particular, if the optical observations start when the reverse shock component still dominates the optical flux, the shape of the optical light curve will appear as case 1 or case 2 in Figure 1. In the first case the light curve will show a transition from steep to shallow power law decay index. In the second case it will show a re-brightening, but if observations do not start early enough the first steep segment (thick dashed line on Figure 1) of the light curve should be missing and it will be visible only in the rise of the forward component. The observed peak in case 2 will correspond to the passage of the $\nu_{\rm m}$ in the observing band. If there is energy injection to the forward shock emission then the light curve should appear as case 3 in Figure 1. This behaviour can be explained by long-lived central engine activity or large dispersion in the distribution of Lorentz factors (Zhang et al. 2006) or related to the time when the energy is transferred from the fireball to the ambient medium (Kobayashi & Zhang 2007).

Within this theoretical framework, we present the analysis of a sample of 63 GRBs

observed with the network of three 2-m telescopes *RoboNet-1.0*[1] (Gomboc at al. 2006), formed by the Liverpool Telescope (LT, La Palma, Canary Islands), the Faulkes Telescope North (FTN, Haleakala, Hawaii) and the Faulkes Telescope South (FTS, Siding Spring, Australia). For those GRBs with detected optical counterparst, we discuss their light curve properties, compare optical and X-ray data and analyse the intrinsic rest frame properties of those bursts with known spectroscopic redshift. An analysis of the bursts for which no afterglow was detected is also presented and discussed within the standard fireball model.

Throughout we use the following conventions : the power law flux is given as $F(\nu, t) \propto t^{-\alpha}\nu^{-\beta}$, where α is the temporal decay index and β is the spectral slope; we assume a standard cosmology with $H_0 = 70$ km s^{-1} Mpc^{-1}, $\Omega_m = 0.3$ and $\Omega_\Lambda = 0.7$; all errors and uncertainties are quoted at the 1σ confidence level.

2. Observations and Analysis

All three telescopes enable rapid response (the typical mean reaction time is $< t > \sim$ 2.5 minutes after the trigger) and deep observations ($R \sim 21$ at $t \sim 5$ minutes after the trigger) to GRB alerts, which are crucial in the case of faint or optically dark bursts. Each telescope operates in a fully robotic mode, responding automatically to a GRB satellite alert by immediately over-riding the current observing programme, then obtaining, analysing and interpreting optical images of the GRB field using the specially designed, sophisticated pipeline (LT-TRAP); subsequent robotic followup observations are then optimised and driven by the automatically derived properties of the afterglow (see Guidorzi et al. 2006). Up to September 2007 the network robotically reacted to 63 GRBs with 24 optical afterglow detections and 39 upper limits (Figure 2).

In this paper, the optical photometry of each optical afterglow was performed using Starlink/GAIA photometry tools. Each field of view was calibrated with the best data available: 1) standards stars observed during the night, if the night was photometric; 2) pre-burst calibration fields (both for SDSS or Bessell filters) reported in GCN Circulars; 3) differential photometry with catalogued stars in the field of view (USNOB1.0 catalogue). This procedure has been followed for all the sample data. All the calibrated magnitudes in the SDSS-r' filter (for all the bursts observed with the LT telescope) were then transformed to the R_C band using the filter transformations given by Smith et al. (2002); the colour term $R - r'$ was then derived for the selected stars used to calibrate the field and finally applied to the estimated magnitude. Data calibration is also discussed in Guidorzi et al. (2005b,

[1] *http://www.astro.livjm.ac.uk/RoboNet/*

2007), Monfardini et al. (2006) and Mundell et al. (2007b).

3. Results

3.1. Optical Detections

The observed optical light curves of the detected afterglows in our sample are shown in Figure 2 (left panel). In the right panel of the same figure all the deep upper limits for the undetected afterglows are shown, using the same scale on the y-axis to emphasize the large range in brightness and time covered by our observations.

The individual light curves of the detected afterglows are then shown in Figure 3, which shows R band observations together with the corresponding *Swift* X-ray light curves. Temporal and spectral properties are summarised in Table 1. We give both temporal and spectral information for each burst, when available. We fitted the data either with a single or with a broken power law; the values reported in the table are the best fitting results. The values reported for $\beta_{\rm O}$, $\beta_{\rm X}$ and $\beta_{\rm OX}$ are retrieved from the literature. In the last two columns of the table we report the redshift (z) and the derived isotropic gamma-ray energy ($E_{\gamma,\rm iso}$) of the burst. For all the bursts detected by the *Swift* satellite the value of $E_{\gamma,\rm iso}$ reported in the table is taken from Butler et al. (2007). For the no-*Swift* bursts we calculated $E_{\gamma,\rm iso}$ assuming a standard cosmology as reported at the end of Section 1, with the following formula: $E_{\gamma,iso} = (4\pi D_L^2\ f)/(1+z)$, where D_L is the luminosity distance and f is the gamma ray fluence of the burst.

Some of the sample bursts have been discussed in previous dedicated papers, but are presented here for completeness. For each burst in our sample we summarise its key properties, together with references to more detailed work where relevant:

- GRB 041006 : this HETE burst was observed with Chandra between 16.8 and 42.5 hours after the burst event, showing a single temporal power law decay, whereas in the optical a break in the light curve at early time was clearly visible. At late time ($> 10^6$ s) the contribution of the underlying supernova emerged (Stanek et al. 2005, Soderberg et al. 2006). The spectral indices in the two bands are consistent, with a slope $\beta_{\rm OX} \sim 0.7$ (Butler at al. 2005; Garnavich et al. 2004). Chandra X-ray data are not shown in our plot; the results of X-ray analysis are taken from Butler et al. 2005.

- GRB 041218 : for this long INTEGRAL burst there is only a late XRT observation. We do not have information for the X-ray temporal decay but in the optical we see a

steepening of the decay after ~ 0.10 days. No spectral information is available for this burst.

- GRB 050502A : for this long INTEGRAL burst the XRT provided only an upper limit for the X-ray flux at ~ 1.3 days. In the optical band the light curve can be described by a single power law with a hint of a bump at 0.02 days. In the X-ray band, temporal and spectral parameters are consistent with similar behaviour to that of the optical (see Guidorzi et al. 2005b for the detailed analysis of this burst).

- GRB 050713A : XMM observations performed between 5.8 and 13.9 hours after the burst, show a break in the X-ray light curve at $\sim 2 \times 10^4$ s. That break is marginally detected in the X-ray data acquired by *Swift*, while the optical light curve is well described by a shallow power law at all times (Guetta et al., 2006). XMM data are not reported in our plot; an accurate spectral analysis has been done by Morris et al. (2007).

- GRB 050730 : both X-ray and optical light curves of this *Swift* burst show a steepening of the initial temporal power law decay at 0.1 days, more pronounced in the X-ray band. The derived spectral slopes from X-ray and optical data are statistically in agreement (Pandey et al. 2006).

- GRB 051111 : the optical light curve is well fitted by a broken power law with an early break around 12 minutes, while in the X-ray no early data were acquired and no break is visible. A comprehensive multi-wavelength temporal and spectral study of this burst has been done by Guidorzi et al. (2007), Yost et al. (2007) and Butler at al. (2006).

- GRB 060108 : this burst has a faint, but relatively blue, optical afterglow that was identified by deep rapid FTN observation, without which it would have been classified as dark burst ($\beta_{\rm OX} \sim 0.5$ and no afterglow was detected by the *Swift* UVOT within the first 300 s). It shows a canonical X-ray light curve while in the optical band the flux may show a similar behaviour but, due to its optical faintness the resultant sparse sampling with co-added images provides a light curve that is consistent wit a single power law. The darkness of this burst can be explained by a combination of an intrinsically optical faintness, an hard optical to X-ray spectrum and a moderate extinction in the host galaxy (Oates et al. 2006).

- GRB 060203 : after an initial rise, the optical light curve follows a shallow power law decay (typical example of the case 2 reported in Figure 1). Due to observing constraints, X-ray observations started only 10^3 s after the trigger and the light curve shows evidence of a power law decay roughly consistent with the optical one. The

spectral fit gives a value of $\beta_X \sim 1.1$ and shows a value of N_H in excess of the galactic one (Morris et al. 2006a).

- GRB 060204B : the early X-ray light curve is dominated by flaring activity and only after 2×10^3 s does the decay appear to be a single power law (Falcone et al. 2006a). In the optical the afterglow is faint and the light curve is a simple power law, shallower than the X-ray decay.

- GRB 060206 : the detailed analysis of the optical light curve showed dramatic energy injection at early time, with at least 3 episodes, with the largest one also visible in the X-ray light curve. At late times a break is evident in the optical but not in the X-ray band; the chromatic nature of the break is not consistent with the possible jet-break interpretation and can be ascribed to a change in the circumburst density profile (Monfardini et al. 2006). In a recent work Curran et al. (2007) found that the data are also consistent with an achromatic break, even if the break in the X-ray is less pronounced. However, the complete X-ray data set acquired with XRT remains consistent with a single unbroken power law decay up to 10^6 seconds (Morris et al. 2006b, Burrows & Racusin 2007) , and the first explanation for the break seems to be the more plausible.

- GRB 060210 : the optical light curve exhibits a power law decay after an initial flat phase ($\alpha = 0.09 \pm 0.05$, case 3 in Figure 1). There is marginal evidence for a break at late times ($t_{O,break} \sim 0.1$ days) but there are not enough optical data to support that. Instead a break is visible in the X-ray light curve, but the late time break is not simultaneous ($t_{X,break} \sim 0.3$ days). We can not exclude the possible achromatic nature of that break due to the very complex behaviour of X-ray light curve.

- GRB 060418 : in the optical and infrared bands (see Molinari et al., 2007 for the infrared analysis) an initial rise is visible, followed by a straight power law decay (case 2 in Figure 1). Fitting the early X-ray data it is possible to see a change in the slope, but, accounting for the presence of a large flare, the data are also consistent with a single power law decay. There is no evidence of temporal break up to 10^6 s in both optical and X-ray bands. The spectrum of the underlying X-ray afterglow can be described by a simple absorbed power law with $\beta_X = 1.04 \pm 0.13$ (Falcone et al. 2006b). The low degree of polarization of the optical light at early time (at ~ 200 s after the event) ruled out the presence of a large scale ordered magnetic field in the emitting region (Mundell et al. 2007a).

- GRB 060510B : the temporal behaviour in the X-ray seems to be the canonical steep-shallow-steep decay with superimposed flares, even if the light curve at late times is

poorly sampled. Looking at the flat light curve at early times, possibly the prompt gamma-ray component is detected in XRT ($T_{90} \sim 280$ s). Due to the high redshift, the optical flux is suppressed by the Lyα absorption and our early optical data are consistent with a single power law decay. No optical observations at late time were available to confirm the possible achromatic nature of the break observed in the X-ray band. The early time X-ray spectrum is well fitted with an absorbed power law with $\beta_X \sim 0.5$ (Perri et al. 2006). This is the value of β_X reported in Table1 because estimated at a time consistent with the time of our optical observations. At late times, taking into account the intrinsic absorption at the redshift of the burst, the spectrum is well fitted by an absorbed power law with $\beta_X \sim 1.5$ (Campana et al., 2006).

- GRB 060512 : optical data are consistent with a single power law. In the X-ray a clear flare is visible at early times and the decay after 10^3 s is a simple power law. At late time, the X-ray spectrum has a slope $\beta_X \sim 0.9$ (Godet et al. 2006).

- GRB 060927 : due to the high redshift ($z = 5.467$), the optical light curve is highly affected by Lyα suppression, particularly in the R filter. The light curve in the I band shows evidence of a possible extra component at early times, but after 500 s the decay is a single power law ($\alpha_I \sim 1.2$). In the X-ray a change of slope is clearly visible and the spectrum is well modelled with an absorbed power law with $\beta_X \sim 0.9$ (Ruiz-Velasco et al., 2007).

- GRB 061007 : the optical light curve exhibits an early peak followed by an unprecedented straight power law decay up to (and likely beyond) 10^6 s after the burst (a good example of case 2 in Figure 1), perfectly mirrored in the X-ray band. The peak at early times can be explained in the context of the fireball model: no optical flash is seen because the typical frequency of the reverse shock emission lies in the radio band at early time and the optical afterglow is dominated by forward shock emission (Mundell et al. 2007b). The broad band optical to γ-ray spectral energy distribution is well described by an absorbed power law with $\beta \sim 1.0$ (Mundell et al. 2007b, Schady et al. 2007).

- GRB 061110B : this burst is intrinsically faint and displays a simple power law decay both in the optical and in the X-ray bands. It showed a typical GRB afterglow spectrum with $\beta_X \sim 1.0$ (Grupe et al. 2006).

- GRB 061121 : this is a perfect example of canonical light curve in the X-ray band not replicated in the optical. The light curve follows a simple power law decay even though the observations began when the initial steep X-ray phase was still ongoing (Page et al., 2007).

- GRB 061126 : the optical light curve shows a steep to shallow transition at about 13 minutes after the trigger. The early, steep component can be interpreted as due to the reverse shock while the later slowly fading component is coming from the forward shock (clear example of case 1 in Figure 1). X-ray observations started after the transition in optical, and show the X-ray afterglow decaying with $\alpha_{X,2} > \alpha_{O,2}$ (faster than the optical afterglow) to the end of observations at 10^6 s (for more details see Gomboc et al. 2008).

- GRB 070208 : after an initial rising phase, the X-ray light curve shows a power law decay. The optical data cover the same time interval as the X-ray data but no rising phase is detected and the optical light curve is well described by a simple power law, after an initial flat phase (case 3 in Figure 1). The optical decay index after the flat phase remains shallower than the decay in the X-ray band.

- GRB 070411 : in this case the temporal decay in the two bands is very similar, but in the optical band an initial rising phase is detected that is not visible in the X-ray band, probably due to the poor sampling at early times in that band. The optical light curve seems to be another example of case 2 reported in Figure 1 but the shape is not smooth and clear, with significant scatter (possibly variability) around the power law decay.

- GRB 070419A : different observations in the optical band show that at early time the afterglow brightened before starting a shallow decay phase that lasts up to 10^6 s. Although the X-ray temporal decay at late time ($\alpha_{X,2} = 0.64 \pm 0.10$) agrees very well with the optical decay ($\alpha_{O,2} = 0.58 \pm 0.04$), at early times the X-ray light curve shows a rapid decay, with no hints of any flare activity. The shape observed in the optical band does not fit the three cases reported in Figure 1 and is probably the result of an episode of energy injection.

- GRB 070420 : another example of canonical light curve in the X-ray band not replicated in the optical. However, in this case the optical light curve is less well sampled than GRB 061121, so it is more difficult to constrain the optical behaviour in the entire time interval covered by XRT observations.

- GRB 070714B : the X-ray data show a steep-shallow-steep decay, not well constrained at late times and with possible small flaring activity. The optical counterpart is very faint but appears to show a shallower power law decay compared with the X-ray decay at late times.

3.2. Optical Upper-Limits

In Table 2 we report the optical upper limits for all the bursts observed with the Liverpool and the Faulkes telescopes for which we did not detect any afterglow candidate. For each GRB we specified when the XRT position for the X-ray afterglow was found. The duration, the BAT fluence f (15-150 keV), the XRT early flux F_X (0.3-10 keV), the time of X-rays observations ($\Delta\ t_X$), the temporal decay (α_X) and the spectral slope (β_X) in the X-ray band, are the values reported in the GCNs or taken from the *Swift* general table. $R^{\rm u.l.}_{\rm start}$ are the values of our optical upper limits at $\Delta\ t_{\rm start}$ minutes from the trigger, where $\Delta\ t_{\rm start}$ is the starting time of our observations. $R^{\rm u.l.}_{\rm mean}$ are the values of our optical upper limits at $\Delta\ t_{\rm mean}$ minutes from the trigger (mean time) for the coadded frames with a total integration time of T_{exp} minutes. The columns OT and A_R show when an optical (O) or infrared (IR) afterglow for that burst had been detected by other facilities and the extinction for the R band in the direction of the burst. The last two columns on the table are the value of the X-ray temporal decay inferred from our fit of the XRT light curves ($\alpha_X^{\rm (fit)}$) and the estimate of the X-ray flux (F_X) at the time of our optical upper limit $\Delta\ t_{\rm mean}$.

X-ray light curves are given in Figure 4 together with our optical upper limit. The best fit for the X-ray light curves is shown. The temporal decay indices in the X-ray band ($\alpha_X^{\rm (fit)}$) reported in Table 2 refer to the segment of the light curve contemporaneous with our optical limit. Only two of the bursts listed in the table were detected by UVOT in the optical bands (GRB 070721A and GRB 070721B); we did not detect the optical counterpart for these two bursts because our observations were performed at late time due to observational constraints.

Of the 39 non-detections, 10 were detected by other facilities, primarily at infrared wavelengths or using larger aperture optical telescopes; the other 29 remain as non-detections. Details are summarised below:

- GRB 050124 : an infrared candidate was detected and confirmed by two Keck observations performed in the K_s band about 24.6 and 47.8 hours after the burst ($\Delta K_s \sim 0.5$, Berger et al. 2005a, Berger et al. 2005b). No afterglow was detected in the optical bands even by the UVOT telescope ($\sim$ 3 hours after the trigger, Lin et al. 2005, Hunsberger et al. 2005). Our observations were performed manually in the R band only after 14.7 hours for observational constraints and no optical counterpart was detected.

- GRB 050716 : our observations in the optical band began 3.8 minutes after the burst with the FTN telescope but no optical candidate was found down to a limit of R$\sim$20 mag (Guidorzi et al. 2005a). A potential infrared counterpart ($J - K \sim 2.5$) was found in UKIRT observations just outside the XRT error circle (Tanvir et al. 2005).

At the position of that candidate we did not clearly detect any source in the R and I bands but we found an excess flux which suggests that the afterglow is probably reddened rather than at very high redshift. A broad-band analysis found that $z \sim 2$ is a good estimate for the redshift of this event and that a host galaxy extinction of $A_V \sim 2.0$ can account for the relatively faint optical/infrared afterglow observed (Rol et al. 2007b).

- GRB 060116 : also for this burst an infrared candidate was detected in UKIRT observations (Kocevski et al. 2006a, Kocevski et al. 2006b). The afterglow of that burst was detected with an unfiltered magnitude ∼20 (Swan et al. 2006) and the very red colours of this afterglow ($J - K = 2.5$, $I - J > 2.9$, Malesani et al. 2006a) suggest the source to be a highly dust extincted ($A_V > 2.5$) but not at high redshift (Tanvir at al. 2006a).

- GRB 060121: the SXC error circle for this HETE-II short burst was partially covered by our first LT observation starting 0.83 hours after the burst. Only in the second observation starting 2.44 hours after the event the XRT error circle was entirely inside our field of view. The detected optical/infrared afterglow (Levan et al. 2006a, Malesani et al. 2006b, Hearty et al. 2006a, Hearty et al. 2006b) is not seen in our images down to a limiting magnitude of $R \sim 22$ at ~ 3 hours after the burst. Subsequent HST observations revealed the presence of a very faint (both in optical and infrared) red galaxy, probably an edge-on disk, close to the position of the afterglow (Levan et al. 2006). In this case this would favour a higher redshift for this burst than has been measured for most short bursts to date.

- GRB 060319 : an infrared candidate was found in WHT observations ($K = 19.0 \pm 0.3$, Tanvir et al. 2006b) but no claims about variability have been made. Our observations set an upper limit of $R \sim 21$ mag after 10 minutes of the burst and no other optical observation detected any possible counterpart down to $R \sim 23$ mag (D'Avanzo et al. 2006a, Lipunov et al. 2006).

- GRB 060602A : a very faint possible optical candidate was detected about 15 minutes after the burst ($R \sim 22.5 \pm 0.3$, Jensen et al. 2006). The transient nature of the source was difficult to assess but was not visible in the SDSS pre-burst image. Our observations were affected by the bright moon and only an upper limit of $R \sim 16.8$ mag was set about 36 minutes after the burst.

- GRB 060923A : an infrared afterglow was detected in the K-band but undetected in I and J bands (Tanvir et al. 2008, Fox et al. 2006a, Fox 2006), suggesting again a highly extinguished or high redshift afterglow for this burst. The subsequent detection

of a faint host galaxy ($R \sim 25.5$, Tanvir et al. 2008) set an upper limit for the redshift of this burst of $z \sim 5$, leaving the extinction as the most likely cause of the extremely red colours measured at early times.

- GRB 060923C : the afterglow of that burst was detected and confirmed in the infrared bands (Covino et al. 2006, Fox et al. 2006b, D'Avanzo et al. 2006b). No indication of any optical identification means again that the possible explanation is a high redshift or high extinction origin for that burst.

- GRB 061006 : a source was found to vary with $\Delta I \sim 0.5$ mag between 0.6 and 1.6 days after the burst in the I-band (Malesani et al. 2006c, Malesani et al. 2006d). This source was identified with the afterglow of this short-hard burst. However the inferred power-law decay slope was quite shallow (~ 0.5) and in the second observation the source was extended so the detection was contaminated by the host galaxy (Malesani et al. 2006d).

- GRB 070223 : the afterglow of that burst was confirmed in the infrared band (Castro-Tirado et al. 2007, Rol et al. 2007) and found to be very faint in the optical band, close to the deep limit of our observations.

In summary, of the 10 afterglows discussed above, 7 were detected in the infrared bands with very red colours and 3 in the optical band. Of those latter 3 optical afterglows, two (GRB 060602A and GRB 061006) had a magnitude below our limiting magnitude in the same band at the same time. For the remaining one (GRB 060121) our observations performed ~ 2.5 hours after the burst support a probable high-redshift nature for this event.

4. Discussion

4.1. A Comparison of X-ray and Optical Light Curves

For a simple visual comparison we show in Figure 3 the X-ray light curves (where data were available, from Evans et al. 2007 [2]), together with the optical light curves, including all published data. When optical and X-ray data cover the same time interval we superimposed on the data a simple power-law fit, to better understand the temporal decay behaviour. As can be seen, the light curves in the two bands do not follow the same temporal decay for

[2]For those bursts where no exact conversion factor from count rate to observed flux (0.3-10 keV) was available we assumed the mean value of 5×10^{-11} erg cm^{-2} s^{-1}.

all the GRBs. For the majority of the bursts the behaviour in the X-ray and optical bands is different, especially at early times where in the X-ray band the temporal decay is steep, showing the hints of large flare activity.

4.1.1. Blastwave Physics from Light Curves Breaks

In the standard fireball model, observed afterglow emission is synchrotron radiation from a quasi-spherical relativistic blast wave (forward shock) that propagates into the homogeneous or wind-like ambient medium. The model can give clear predictions of the shape of light curves at different frequencies. Here we test this model comparing the theoretical expectations with the observed light curves properties. We take into account simple modifications to the standard model if needed. The modifications are energy injection into the blast wave in the afterglow phase ($L \propto t^{-q}$) and a generalized wind environment ($\rho \propto R^{-s}$). The injection would modify the bast wave dynamics as long as $q < 1$ and $q = 1$ corresponds to the case without energy injection. The possible theoretical values for the temporal decay index α and the spectral index β as functions of the electron spectral index p are summarized in Table 3.

Traditionally, optical data from ground based telescopes alone have been used to establish the presence of achromatic breaks since the number of pre-*Swift* bursts with good simultaneous X-ray and optical data at any time (early and late) was very small. However, recent studies of *Swift* bursts have shown that many *Swift* GRBs exhibit a well defined steepening of the X-ray light curve while the optical decay continues to be described by a single un-broken power law (Panaitescu et al. 2006). In some cases the decay is a straight power law at all times with no breaks either in the optical or in the X-ray band (Mundell et al. 2007b), while in some bursts the break is observed only in the optical but not in the X-ray band.

In this paper we study breaks in X-ray and optical light curves in the decay phase. Immediately after the prompt emission, some light curves show a peak or flare features which are likely to be due to central engine activity or reverse shock emission. We concentrate our discussion on the study of simpler forward shock emission. The bursts in our sample (see Figure 3) can be divided into four main classes, depending on the presence or not of a break in the optical curve (see Figure 5):

- Class A : no break in the optical or in the X-ray band;
- Class B : no break in the optical band, break in the X-ray band;

- Class C : break in the optical band, no break in the X-ray band;
- Class D : break in the optical and in the X-ray band.

In the cartoon shown in Figure 5 we show the shape of the four classes. This classification is based on the available data in the two bands: *Swift*-XRT for the X-ray light curve and our telescopes, GCNs and published data for optical light curves. There is clearly the possibility of additional breaks in the period not covered by the observations both in the optical and in the X-ray band. The possible mechanisms that can produce a break in the observed light curves in the decay phase can be summarised as follow:

1. the cooling break → chromatic break;
2. cessation of energy injection → achromatic break;
3. jet break → achromatic break;
4. change in the ambient distribution → chromatic or achromatic break;
5. additional emission component (reverse shock, late central engine activities, SN-component, host galaxy contamination) → chromatic break;

In the epoch under investigation in this paper ($10^2 - 10^6$ s), the emission process is in the slow cooling regime. One of the most natural explanations for a break in a light curve is the cooling break (i): on the passage of the cooling frequency through the observation band, the light curve steepens by $\delta\alpha = 1/4$. The steepening happens in the X-ray band first and in the optical band later for a homogeneous medium, while it occurs in the optical band first and in the X-ray band later for a wind-like medium. Note that the cooling frequency increases in time for the wind-like medium. The cessation of energy injection into the blast wave (ii) or a jet break (iii) causes a change in the hydrodynamics of the blast wave, producing achromatic breaks in the light curves. In the post-break phase, the optical and X-ray decay indices could be the same or different by $\alpha = 1/4$ for mechanism (ii). The decay indices in the two bands should be the same for a jet break (iii). It should be noted that for the mechanism (iv) the afterglow emission above the cooling frequency does not depend on the ambient matter density. The break is achromatic if the cooling frequency is located above the X-ray band, while it is chromatic if the cooling frequency lies between the two bands. The mechanisms (v), especially reverse shock emission and late time internal shocks, are generally believed to be relevant only at early times and their contribution to the shape of the light curves becomes negligible at late times.

Temporal and spectral properties of all the bursts in the sample are reported in Table 1. Assuming the standard fireball model and a homogeneous or wind-like circumburst medium it is possible to derive the closure relations between the temporal decay index (α) and the spectral slope (β) in order to satisfy the models (e.g. Zhang et al. 2006). In Figure 6 the comparison between observed properties and model expectations is shown in the optical (left panel) or in the X-ray (right panel) band. The two bursts indicated on the left panel of Figure 6 (GRB 060108 and GRB 060210) are the ones that, based on the optical data, deviate the most from the standard model. In the case of GRB 060108 the spectral optical analysis (without accounting for extinction) gives a steep value for $\beta_{\rm O}$, hard to explain for the standard model. When extinction is included a shallower value is found ($\beta_{\rm OX} \sim 0.5$) more in agreement with the observed spectral energy distribution (Oates et al. 2006). For GRB 060210, the spectral analysis reveals a large difference between $\beta_{\rm X}$, $\beta_{\rm O}$ and $\beta_{\rm OX}$, probably due to a large amount of extinction which is difficult to evaluate. If again we consider the value found from the fit of the multiband spectral energy distribution a value in agreement with the model is found (see Curran et al. 2007 for detailed analysis of this burst). Using temporal and spectral information (when available), it is now possible to constraint the value of electron spectral index (p) for different bursts and study each burst belonging to our four classes in the context of the standard fireball model.

4.1.2. Class A - no breaks

For 10 bursts (GRB 050502A, GRB 060203, GRB 060204B, GRB 060418, GRB 060512, GRB 061007, GRB 061110B, GRB 070208, GRB 070411 and GRB 070419A) no break is observed in the optical or X-ray bands, but in general, the decay indices of the optical and the X-ray light curves are different.

The simplest explanation for the difference is that the cooling frequency is situated between the optical and the X-ray band. If this is the case, the difference is $\delta\alpha = 1/4$ as we have discussed in the previous section. If there is energy injected into a blast wave $L \propto t^{-q}$, the difference is given by $\delta\alpha = (2-q)/4$ (see Table 3). The X-ray light curve is steeper by $\delta\alpha$ than the optical in the homogeneous medium, while the optical one is steeper by $\delta\alpha$ in the wind-like medium. In the generalized wind-like medium case $\rho \propto R^{-s}$ (with no energy injection), optical afterglow decays faster by $\delta\alpha = (3s-4)/(16-4s)$ than the X-ray afterglow (Monfardini et al. 2006).

- GRB 050502A : the decay index of the X-ray afterglow is not well determined, and late time *Swift* observations give only a lower limit for $\alpha_{\rm X}$. Since the optical decay is shallower, $\nu_{\rm c}$ should lie between the two bands and the homogeneous ambient medium

is favored. The electron spectral index is given by $p = 2\beta_X = 2.6 \pm 0.3$. The theoretical values $\alpha = 3(p-1)/4 = 1.2$ and $\beta = (p-1)/2 = 0.8$ are in good agreement with the observations (Guidorzi et al. 2006).

- GRB 060203 : the X-ray light curve is steeper by $\delta\alpha \sim 0.2$ than the optical light curve. It indicates the uniform ambient medium and $\nu_O < \nu_c < \nu_X$ during the power law decay phase. The theoretical estimates $\alpha_O \sim 0.75$, $\alpha_X \sim 1.0$ and $\beta_X \sim 1.0$ ($p \sim 2.0$) can explain well the observations ($\alpha_{O,1} = 0.74 \pm 0.13$, $\alpha_{X,1} = 0.94 \pm 0.05$ and $\beta_X = 0.9 \pm 0.2$).

- GRB 060204B : the X-ray afterglow decays faster by $\delta\alpha = 0.62$ than the optical afterglow. The difference $\delta\alpha$ is larger than the value $\delta\alpha = 1/4$ for a simple model in which the optical and X-ray bands are in different spectral domain (i.e. $\nu_O < \nu_c < \nu_X$). Since X-ray light curve is steeper than the optical light curve, wind-like medium model does not work. Although constant energy injection (q=0) gives a close value $\delta\alpha = 0.5$ we do not expect the observed steep decay $\alpha_{O,1} = 0.73$ and $\alpha_{X,2} = 1.35$ for such significant energy injection. In the early phase flares are noticeable in the X-ray light curve. Late internal shock emission might dominate X-ray band at later times as well. Superposed flares might steepen the X-ray light curve. Another possible explanation is that fluctuations in the ambient medium produce bumps in the late optical light curve (this interpretation was already proposed by Guidorzi et al. 2006 to explain the bump in the light curve observed for GRB 050502A). If the cooling frequency lies between the two bands, the bumps are produced only in the optical light curve. Since the optical observations are very sparse for this afterglow,a bump in the optical light curve might take the decay index shallower than the real value.

- GRB 060418 : the X-ray light curve is steeper by $\delta\alpha = 0.25$ than the optical light curve in the late decay phase. This indicates an uniform ambient medium with $\nu_O < \nu_c < \nu_X$ during that phase. Temporal observed values ($\alpha_{O,1} = 1.19$, $\alpha_{X,1} = 1.44$) are in agreement with the theoretical expectation of a simple model with a value for the spectral index of $p \sim 2.6$ ($\alpha_O = 1.20$, $\alpha_X = 1.45$).

- GRB 060512 : the X-ray emission decays faster by $\delta\alpha = 0.38$ than the optical emission. The difference $\delta\alpha$ is not consistent with the simplest scenario ($\delta\alpha = 1/4$). The energy injection (q=0.48) in homogeneous ambient can account for the large value of $\delta\alpha$. However, even with $p = 2\beta_X = 2.2$, the maximum value allowed from the observed spectral index $\beta_X = 0.93 \pm 0.18$, the expected decay indices $\alpha_O = [(2p-6)+(p+3)q]/4 = 0.22$ and $\alpha_X = [(2p-4)+(p+2)q]/4 = 0.60$ (Zhang et al. 2006) are much shallower than the observed values. X-ray flares might make the X-ray decay index larger than the real decay index of the blast wave emission.

- GRB 061007 : the afterglow of this burst is very bright in optical and X-ray, the decay is a straight power law from early time (there is the hint of a rise in the optical not mirrored in the X-ray) since late times. A comprehensive multiwavelength analysis of this burst is presented in Mundell et al. (2007b): the evolution of the afterglow can be explained in the context of the fireball model with $\nu_{\rm m} < \nu_O < \nu_{\rm X} < \nu_c$ for the entire 10^6 s period covered by the observations.

- GRB 061110B : for that burst the optical light curve decays faster by $\delta\alpha = 0.20$ than the X-ray, indicating that during the observations $\nu_{\rm c}$ is located between the two bands in a wind-like medium. The X-ray data imply a value of $p \sim 2.5$ and the expected value for the optical temporal decay $\alpha_{\rm O} \sim 1.63$ is in good agreement with that observed ($\alpha_{\rm O,1} = 1.64 \pm 0.08$).

- GRB 070208 : the X-ray afterglow decays faster by $\delta\alpha = 0.87$ than the optical afterglow. Again this difference is much larger than the value $\delta\alpha = 1/4$ for a simple model, similar to the case of GRB 060204b. Also the energy injection model can not account for the larger value $\delta\alpha = 0.87$. Beyond the standard model, possible explanations of such a large difference are X-ray flares (late time internal shocks) which make the X-ray steeper coupled with energy injection which makes the optical decay shallower.

- GRB 070411 : the X-ray afterglow decays faster by $\delta\alpha = 0.20$ than the optical afterglow. It indicates the uniform ambient medium and $\nu_{\rm O} < \nu_{\rm c} < \nu_{\rm X}$ during the power law decay phase. If this is the case, the value of p derived from the X-ray data ($p \sim 2.2$) imply a value of the decay indices $\alpha_{\rm O} \sim 0.9$ and $\alpha_{\rm O} \sim 1.2$, well in agreement with the observed values ($\alpha_{\rm O,1} = 0.92 \pm 0.04$ and $\alpha_{\rm X,1} = 1.12 \pm 0.03$).

- GRB 070419A : for this burst the temporal decay in the two bands is again very similar, but this is true only at late times ($\delta\alpha_A = 0.06$), while at early times the shape in the two bands is very different: a very steep decay in the X-ray ($\alpha \sim 2.8$) and a possible broad re-brightening in the optical. Even in the late power law phase, no closure relations for the simple models can reconcile the observed value $\alpha_{\rm X} - 3\beta_{\rm X}/2 = -1.6$. Assuming $\nu_{\rm X}, \nu_{\rm O} > \nu_{\rm c}$ (then the emission does not depend on the ambient medium) we obtain $p = 2.9$ from $\beta_{\rm X}$. The observed decay indices in the two bands ($\alpha_{\rm O} \sim \alpha_{\rm X} \sim 0.6$) and the closure relation could be explained if there is significant energy injection ($q = 0.12$). The total injected energy increases by a factor $(3 \times 10^6/3500)^{(1-q)} = 380$ between the break time $t_{{\rm X},break} \sim 0.04$ days~ 3500 s and the end of the observations $\sim 3 \times 10^6$ s. This could contradict with the energy budget of the central engine (solar mass scale).

4.1.3. Class B - break in the X-ray band only

A steepening in the X-ray decay slope is observed in eight bursts of our sample (GRB 050713A, GRB 060108, GRB 060210, GRB 060510B, GRB 060927, GRB 061121, GRB 070420 and GRB 070714B), while the rate of the optical decay remains constant.

A simple explanation of this behaviour could be the passage of the cooling frequency through the X-ray band. For a homogeneous ambient medium, the decay indices of the optical and X-ray light curves should be the same in the pre-break phase, with only the X-ray light curve steepening due to the passage of ν_c. In contrast, for wind-like medium the optical light curve is steeper than the X-ray light curve in the pre-break phase and the decay indices in the two bands become the same after a break in the X-ray light curve. For the eight bursts in that class, the observed steepening $\delta\alpha$ is always larger than the value $\delta\alpha = 1/4$ expected in the simplest scenario.

- GRB 050713A : the X-ray emission decays faster by $\delta\alpha \sim 0.7$ than the optical in the post-break phase. The decay indices in the pre-break phase are also significantly different from each other ($\delta\alpha = 0.54$). We cannot explain the break (and the behaviour of the light curves in the two bands) by the cooling break even if the energy injection and generalized wind-like medium are assumed. The cessation of the energy injection and a jet break also cannot account for the observed break because of their achromatic nature. The most likely explanation is that X-ray flares due to late internal shocks shapes the X-ray light curve (there are notable fluctuations in the X-ray light curve). Although the optical light curve is poorly sampled, the rather shallow observed decay ($\alpha_{O,1} = 0.63 \pm 0.04$) might indicate energy injection into the blast wave.

- GRB 060108 : the decay indices of the optical and X-ray light curves are almost the same in the pre-break phase, but the steepening in the X-ray band ($\delta\alpha = 0.69$) is too large to be explained in a simple cooling break model (also reported by Oates et al. 2006). Since there are no optical observations at late times, achromatic break mechanisms are also applicable to this event. The X-ray decay after the break ($\alpha_{X,2} = 1.15$) is too shallow for the jet break model in which the electron spectral index should be equal to the post-break decay index ($p = \alpha_{X,2}$ in that case). Considering the shallow pre-break decay in the X-ray and optical, the probable explanation is the energy injection ceasing.

- GRB 060210 : the optical light curve is complex. The early flat portion might be due to energy injection or to the passage of the typical frequency through the optical band, and there is a hint of a late break. Since we are interested in breaks in the decay

phase, we discuss the intermediate power law part of the optical light curve together with X-ray observations. Before the X-ray break the optical afterglow decays faster ($\delta\alpha = 0.15$) than the X-ray afterglow. This could indicate that the cooling frequency lies between the two bands and that the ambient medium is wind-like. Since after the break the X-ray light curve becomes steeper than the optical, the steepening is not explained by a cooling break even if we consider energy injection or a generalized wind-like medium. The post-break X-ray index ($\alpha_{\rm X,2} = 1.31$) is too shallow to be explained in the jet break model. In the model of cessation of energy injection the difference of the decay indices in the two bands ($\nu_{\rm O} < \nu_{\rm c} < \nu_{\rm X}$) is $\delta\alpha = (2-q)/4$in the pre-break phase (during the energy injection) and the steepening in the X-ray light curve (ceasing of energy injection) is given by $\delta\alpha_{break} = (p+2)(1-q)/4$. The observed difference $\delta\alpha = 0.15$ is smaller than the expected value in the energy injection model (q should be smaller than unity). The X-ray spectrum $\beta_{\rm X} = 1.14$ and the observed steepening $\delta\alpha_{break} = 0.43$ require $p = 2.8$ and significant energy injection ($q = 0.60$), for which the decay indices are expected to be $\alpha_{\rm O,1} = 1,13$, $\alpha_{\rm X,1} = 0.78$, $\alpha_{\rm X,2} = 1,21$. This could marginally explain the observations. A more plausible explanation is that X-ray flares due to late central engine activity shape the X-ray light curve.

- GRB 060510B : in the pre-break phase, the decay indices in the two bands are the same if the prompt emission and X-ray flares at early times are ignored. Considering the shallow pre-break decay in the X-ray and optical bands, a possible explanation for the X-ray break is the cessation of energy injection. If this is the case, the optical light curve should have a break at the same time, although there are no optical observations at late times.

- GRB 060927 : the optical light curve in the R-band does not show a simple decay; $\alpha_{\rm O,1} > \alpha_{\rm X,1}$ and $\delta\alpha > 1.0$. There is a possible flat phase in the optical between 10^2 and 10^3 s. A possible explanation could be late energy injection but this behaviour is not mirrored in the X-ray band. The observed characteristics of this burst are difficult to explain in the context of the standard model.

- GRB 061121 : Page et al. (2007) found that the decay indices in the optical and X-ray bands are consistent, within the uncertainties, with the (possible) presence of an achromatic break. However, the optical data after the break, as reported in our Figure 3, are in very good agreement with the same power law decay index observed before the break ($\alpha_{\rm O,1} = 0.83$), without requiring any break in the optical. The chromatic nature of the break excludes the possibilities of a jet break and cessation of energy injection for the explanation of the break in the X-ray light curve. Since the X-ray decay index evolves from almost zero (flat) to a steep value ($\alpha_{\rm X,2} = 1.58$), which is much larger

than the optical decay index ($\alpha_{O,1} = 0.83$), neither cooling break models nor change of the ambient density distribution (e.g. change from ISM medium to wind-like medium during the propagation of the blast wave) can explain the evolution of the X-ray light curve. The emission from late central engine activities could mask the X-ray radiation from the forward shock. The darkness $\beta_{OX} = 0.53$ might be due to the bright additional X-ray emission from the central engine.

- GRB 070420 : the observed data are not consistent with any closure relation for the standard model. The behaviour of the X-ray and the optical light curves looks quite different. However, the sparse observations can not exclude the presence of a flat phase in the optical light curve as visible in the X-ray. If this is the case, the ceasing of energy injection could explain the X-ray and optical observations.

- GRB 070714B : similarly to GRB 070420, the behaviour or the X-ray and optical light curves cannot be explained in the standard model if a single power law is assumed for the decay of the optical light curve. Although the optical data are too sparse to firmly constrain the behaviour in that band, but a possible initial flat phase may be present (like in the X-ray band) followed be a standard power law decay. Like the previous case, the ceasing of energy injection could explain the X-ray and optical behaviours.

4.1.4. Class C - break in the optical band only

In five cases a change of decay index is detected only in the optical light curve and not in the X-ray band (GRB 041006, GRB 041218, GRB 051111, GRB 060206 and GRB 061126).

A possible explanation for these breaks is the passage of ν_c through the optical band. If a homogeneous medium is assumed, the decay indices of the optical and the X-ray light curves should be the same in the post-break phase, with only the optical light curve steepening with the passage of ν_c. If a wind-like ambient medium is assumed, the decay indices in the two bands are the same in the pre-break phase and the optical light curve is steeper than the X-ray after the break.

- GRB 041006 : counting the rather large error in the value of α_X, the X-ray decay and the post-break optical decay indices could be considered as almost the same. If the cooling break model is assumed to explain the steepening of the optical light curve, a homogeneous ambient medium is favored, because the decay indices in the two bands are the same in the post-break phase. The drastic steepening in the optical light curve ($\delta\alpha = 0.53$) requires almost constant energy injection ($q \sim 0$). It is hard to achieve the

steep decay in the post-break phase ($\alpha_{\rm O,2} = 1.12$) with such a massive energy injection. The cooling break model does not work. Since there are no X-ray observations at early times, achromatic break models are acceptable. The post-break optical index is too shallow to consider a jet break.

Next we consider the cessation of energy injection. From the observed spectral indices ($\beta_{\rm O} \sim \beta_{\rm X} \sim 1.0$), the two bands should be in the same spectral domain and we obtain $p \sim 3$ for $\nu_{\rm m} < \nu_{\rm obs} < \nu_{\rm c}$ or $p \sim 2$ for $\nu_{\rm c} < \nu_{\rm obs}$. The closure relations are marginally satisfied in both cases. The ceasing of energy injection causes steepening in a light curve. If the observation band is above $\nu_{\rm c}$ the flux does not depend on the ambient medium and the steepening is $\delta\alpha = (p+2)(1-q)/4$. If $\nu_{\rm m} < \nu_{\rm obs} < \nu_{\rm X}$ the steepening is $\delta\alpha = (p+3)(1-q)/4$ for a homogeneous ambient medium and $\delta\alpha = (p+1)(1-q)/4$ for a wind-like ambient medium. For the combination of $\nu_{\rm m} < \nu_{\rm obs} < \nu_{\rm c}$ and homogeneous ambient medium, the initial energy injection is mildest $q = 0.47$ and the expected values $\alpha_{\rm pre-break} \sim 0.71$, $\alpha_{\rm post-break} \sim 1.5$ and $\beta \sim 1.0$ could be consistent with the observations.

- GRB 041218 : there is only a late time observation for the X-ray band, neither $\alpha_{\rm X}$ nor $\beta_{\rm X}$ are constrained from the observations. The optical spectral index $\beta_{\rm O}$ is also not available. The break in the optical light curve ($\delta\alpha = 0.22$) could be explained in many models including the cooling break.

- GRB 051111 : since the X-ray decay index $\alpha_{\rm X,2} = 1.60$ is incoincident with both the pre-break ($\alpha_{\rm O,1} = 0.82$) and the post-break ($\alpha_{\rm O,2} = 1.0$) optical decay index, cooling break models cannot account for the optical break even if energy injection is considered. The fact that the X-ray emission decays faster than the optical emission rules out a wind-like ambient medium scenario (and scenarios related to the wind medium). No X-ray observations are available before the optical break and the break might be achromatic. The jet break is unlikely because the afterglow decays with significantly different rates in the two bands after the break. The difference of the spectral indices in the two bands indicates that the two bands are in different spectral domains (i.e. $\nu_{\rm m} < \nu_{\rm O} < \nu_{\rm c} < \nu_{\rm X}$). This highlighted by the spectral energy distribution analysis presented in Guidorzi et al. 2007. Using the observed $\beta_{\rm O} = 0.76$ (for which the error is smaller than in $\beta_{\rm X}$), we obtain $p = 2\beta_{\rm O} + 1 = 2.5$. If the energy injection rate changes from q_1 to q_2 at the break, the steepening of the optical decay is given by $\delta\alpha_{\rm O} = (p+3)(q_2 - q_1)/4 = 0.18$ and the difference of the decay indices is $\delta\alpha = (2 - q_2)/4 = 0.6$ in the post-break phase. The resulting q_1 and q_2 are negative and unphysical, with which the predicted temporal and spectral indices deviate largely from the observed values. The energy injection model also does not work.

- GRB 060206 : the X-ray light curve is consistent with a single unbroken power law, achromatic break models (i.e. jet break and ceasing of energy injection) are ruled out. Since the X-ray decay index ($\alpha_{\rm X,1} = 1.30$) is different from both the pre-preak ($\alpha_{\rm O,1} = 0.93$) and the post-break ($\alpha_{\rm O,2} = 1.83$) optical decay indices, the cooling break models can not account for the optical break even if the energy injection or generic wind-like ambient medium is considered. The observed behaviour of the light curves might be due to a transition in the ambient matter distribution (Monfardini et al. 2006): a blast wave initially propagates into a constant medium and then it breaks out into a wind-like medium. Note that X-ray emission does not depend on the ambient matter density (and its distribution) as long as the X-ray band is above the cooling frequency, and that the optical emission (below $\nu_{\rm c}$) reflects the change in the ambient matter distribution.

- GRB 061126 : for this burst no break is visible in the X-ray band, while in the optical the transition is from steeper to shallower decay index. This behaviour at early times can be explained as the contribution from the reverse shock component. The detailed study by Gomboc et al. (2008) shows its inconsistency with the standard fireball model (the steeper decay in the X-ray band and the large ratio of X-ray to optical flux).

4.1.5. Class D - break in both bands

The bursts belonging to this class are those showing a break in both the optical and the X-ray light curves in their decay phases. In general, breaks in the two bands occur at different times, both chromatic and achromatic breaks are considered. Surprisingly, for only one burst do we observe a break in both bands, although GRB 060210 might be classified in this case if we take seriously the last optical data points.

- GRB 050730 : if a jet break is responsible for the steep X-ray decay, the electron energy index is $p = \alpha_{\rm X,2} = 2.37$. Given that X-ray band is below the cooling frequency, the observed X-ray spectral index $\beta_X = 0.73 \pm 0.07$ is consistent with the model prediction $\beta = (p-1)/2 = 0.69$. However, the much shallower optical decay ($\alpha_{\rm O,2} = 1.55 \pm 0.08$) is inconsistent with the jet break model. As pointed out by Pandey et al. (2006), the possibility of a contribution from the host galaxy or an associated SN to the late time optical afterglow can be ruled out considering the high redshift of the burst ($z = 3.967$). Since after a jet break a forward shock emits photons practically at a constant radius (the exponential slowing down; Sari, Piran & Halpern 1999), fluctuations in the ambient medium do not seem to affect the decay rate of the emission. Even if there

is an effect, both light curves should become shallower (or steeper) in the same way because both optical and X-ray bands are in the same spectral domain ($\nu_O, \nu_X < \nu_c$). Energy injection into a forward shock also cannot explain the shallow optical decay because of the same reason. Additional emission components, e.g. the two component jet model or late time internal shocks might make the optical decay slower. The early shallow decay phase observed in the optical and X-ray light curves could be explained by energy injection (Pandey et al. 2006), though the ceasing of the injection should happen around the time of the jet break.

4.1.6. Summary of Light Curves Breaks

From this analysis of the optical and X-ray light curves we conclude that in our sample of 24 optical GRB afterglows: 15 bursts can be explained in the context of the standard fireball model (with modifications: energy injection or variation in the ambient matter distribution); while for the remaining 9 bursts:

- Class A : GRB 060204B, GRB 060512, GRB 070208, GRB 070419A
- Class B : GRB 050713A, GRB 060927, GRB 061121
- Class C : GRB 051111, GRB 061126

the observed data are inconsistent with the predictions of the standard model.

4.2. Rest Frame Properties

In Figure 7 we translate the observed magnitudes of the optical afterglows into the rest-frame luminosity (left panel). The subscript t used in this section refers to the time in the rest frame of the GRBs. We assumed a standard cosmology (defined in Section 1) and we include any correction expected from the distance of the event (z) and its spectral properties (β) in order to report all the observed quantities in the rest frame of the GRB. We corrected the optical magnitude for Galactic extinction using the reddening maps of Schlegel et al. (1998) and we applied the k-correction to take into account the fact that sources are observed at different redshifts ($k = -2.5\ log(1+z)^{(\beta-1)}$). We do not correct for the host galaxy dust absorption. From this analysis we excluded : 1) the bursts for which no spectroscopic redshift was available (GRB 041218, GRB 050713A, GRB 060108, GRB 060203 and GRB 060204B);

2) GRB 060510B, for which there is a value of the spectroscopic redshift but the optical light curve is sparsely sampled. After this selection our sub-sample totals 16 objects.

Even in the rest frame of the burst, starting the observations about 0.5 minutes after the burst event, a difference of about 4 orders of magnitude in luminosity is evident, particularly at early time. This spread in intrinsic luminosity remains after including all the available early and late time public data, although there is a hint of a convergence at later times. It should be noted that our analysis does not take into account any beaming effect. This collimation correction is known to reduce the observed spread in luminosity for bursts (Frail et al. 2001, Panaitescu & Kumar 2001) but requires a correct determination of the jet opening angle for each burst based on an unambiguous identification of a jet break. Identification of such break times is clearly important but, as discussed in Section 4.1.1 is non-trivial due to complex light curve properties and requires well-sampled optical and X-ray light curves from the earliest to the latest possible times.

In a previous study of optical afterglow light curves, Liang & Zhang (2006, hereafter LZ06) suggested that the optical luminosity at t=1 day (source frame time) after the burst shows a bimodal distribution, with a separation at $L^*_{\rm t=1day} = 1.4 \times 10^{45}$ erg s^{-1}. The majority of the bursts in their sample (44 bursts in total) fall into the luminous group (34 bursts with $L_{peak} > L^*_{t=1day}$). Kann et al. 2006 and Nardini et al. 2006 (hereafter K06 and N06 respectively) found a similar result. LZ06 selected t=1 day as the reference time because at this time the light curves of their sample were better sampled. Moreover they selected this late time because they were concerned about the possible contribution of the reverse shock component or additional energy injection at early times. The result of N06 was obtained in the same way but extrapolating the luminosity at t=0.5 days (source frame time).

As our observations have good coverage starting at earlier time (between 1 and 20 minutes in the GRB rest-frame) we have estimated the intrinsic optical luminosity at three different times: 10 minutes, 0.5 days and 1 day (source frame time). In the cases presented here we have confirmed that the reverse shock component does not affect our analysis. As discussed in the previous section, in only one case (GRB 061126) do we detect the possible contribution of the reverse shock at early times. Our early observations at t=10 minutes are more directly related to the explosion energy during the prompt emission phase.

In Table 4 we report the mean values for the rest-frame luminosity calculated at different times. The two classes defined by LZ06 (dim and lum) are not consistent with a single population, as clear from their Figure 2. Our data (at any times) are consistent within the uncertainties with a single population rather than with two separate classes. In Fig 8 we show the observed luminosity distribution of our sample extrapolated at 12 hours.The distribution is well fitted with a single log-normal function with an average of 29.54 ± 0.07

and a σ of 0.67 ± 0.05.

Figure 7 (right panel) shows the luminosity-redshift distribution for the bursts in our sample. In this figure we over plot the separation line between the two classes and the highest values for the redshift of the members of the two groups in the LZ06 sample. As pointed out by LZ06, a possible reason for the lack of high redshift members in their dim group is a lack of deep and rapid followup observations. The burst population detected by *Swift* has a larger mean redshift and fainter brightness distribution that previous missions ($< z >_{Swift} \sim 2.7$, $< z >_{pre-Swift} \sim 1.5$, Le & Dermer 2007). This could explain the results of LZ06, whose sample was based on bursts detected up to August 2005, thus containing only 7 *Swift* bursts. The study presented by K06 of a sample of 16 pre-*Swift* bursts similarly probed the bright end of the GRB luminosity function and found similar conclusions to LZ06. K06 found that on average low-redshift afterglows are less luminous than high-redshift ones, suggesting a bimodal luminosity distribution. Strong selection effects due to observational bias against intrinsically faint afterglows at higher redshifts is a likely explanation for this result. This observational bias is greatly reduced in our sample thanks to the rapid response and use of red filters on our ground based telescopes to *Swift* triggers (14/16 objects used for this analysis were detected by *Swift*). Our results show that faint *Swift* GRBs at higher redshift are readily detected with such rapid, deep optical observations in red filters (Figure 7, right panel), a region of parameter space not accessible in the samples of LZ06 or K06.

The population that is not prevalent in the right panel of Figure 7 is bright bursts at low redshifts, probably due to the GRB luminosity function such that very luminous bursts rare and a large survey volume is therefore required to detect them. Other authors discuss the possibility of two separate luminosity functions for luminous and underluminous GRBs (Nardini et al. 2007, Kann et al. 2007, Liang et al. 2007, Chapman et al. 2007) but given the many complex instrumental selection effects inherent in GRB discovery and followup, significantly larger samples are required to draw robust conclusions. Lower *Swift* trigger thresholds may provide the basis for such samples in the future.

4.3. Dark Bursts

We consider as an optically dark event, or "dark burst" to be a one that satisfies the definition of Jakobsson et al. (2004), i.e. that the slope of the spectral energy distribution between the optical and the X-ray band or spectral index $\beta_{\rm OX}$, is < 0.5. Even optically detected bursts may be classified as "dark", providing that the optical flux is much fainter than expected from scaling the X-ray flux (e.g. GRB060108). For all the bursts reported in Table 2 no optical counterpart was detected by our telescopes. Apart from a few cases in

which our observations were performed at late times, the majority of GRBs in our sample were observed by our telescopes reacting rapidly and performing deep, early-time optical observations ($R \sim 21$ at 5 minutes after the trigger, for co-added images). A late response or poor sensitivity are therefore ruled out as explanations for non-detections in most cases. What, therefore, is the explanation for the lack (or faintness) of the optical afterglow for these 'dark' bursts? To understand this we analyse the X-ray light curve of the bursts in our sub-sample observed by the *Swift*-XRT. Using the decay inferred from the fit of the light curves the X-ray and optical fluxes are extrapolated to a common time. We assume that the optical light curves for those undetected bursts follow a power law decay with a slope equal to the mean temporal decay of the detected afterglows analysed in Section 3 ($< \alpha_{\rm O} > \sim 1.1$). Alternatively, in the X-ray band we use the value derived from the fit of the light curve and reported on Table 2 ($\alpha_{\rm X}^{\rm (fit)}$). Three characteristic times t_0, t_1 and t_2 are used here. The time $t_2 = 11$ hours is chosen for consistency with the dark burst classification of Jakobsson et al. (2004), while fluxes extrapolated to $t_1 = 1$ hour and $t_0 = 10$ minutes exploit our early-time data without compromising observing sensitivity.

As can be seen in Figure 9, the majority of the bursts are located close to the dark bursts region ($\beta_{\rm OX} < 0.5$) independent of the selected time, ruling out late observation time as an explanation for the apparent darkness of most bursts. For almost all the bursts, the evolution of the optical and X-ray flux follows a line almost parallel to the lines of constant $\beta_{\rm OX}$ (bottom right panel). This behaviour can be seen, in the optical band, as a consequence of the assumption of an average decay when making the extrapolation. Any change in the temporal decay would clearly modify this behaviour. However, it seems that bursts that are classified as "normal" after 10 minutes (bottom left panel) remain in the same class also after 11 hours (top left panel). At the same time those bursts that are optically dark soon after 10 minutes belong to the class of the so-called "dark bursts" also after 11 hours.

In only five cases, does the classification of the burst depend on the time for the extrapolation of the flux. For these five bursts we report also the errors (including the uncertainties on the flux and on the α used for the extrapolation) in the bottom right panel of Figure 9. Three bursts are classified as normal bursts if we extrapolate at $t=t_2$ but belong to the class of "dark bursts" if we extrapolate at $t=t_0$ (GRB 050124, GRB 060901 and GRB 070721B, red circles on Figure 9); in two cases it is the contrary (GRB 050504 and GRB 070219, blue circles). In the latter cases it is clear that the optical flux significantly suppressed compared to the X-ray flux. This may be due to spectral evolution of those bursts, but within the uncertainties we cannot rule out the possibility that nothing changes also for these five bursts.

For 10/39 bursts, as reported in Table 2, an optical/infrared counterpart was identified

by larger optical or IR telescopes, with counterparts detected primarily at NIR wavelengths. Our observations rule out the large population of bright optical counterparts that were predicted, pre-*Swift*, to exist and be observable with suitably rapid followup observations. Explanations for dark bursts in the era of rapid followup remain: extinction caused by dust (Galactic or host), high redshift origin, or both. In some cases ($\sim 10\%$) the Galactic absorption along the light of sight in the observing band (A_R) for our bursts is significant and may explain the undetected optical counterpart; however, it is interesting to note that no IR detections have been reported for these GRBS. The effect of Ly-α absorption due to an high-redshift event ($z > 7$) is difficult to evaluate but again this effect could be responsible at least for a fraction of our non-detections (Roming et al. 2006). The possibility of a rapid temporal decay seems to be the most unlikely: in fact, assuming that the undetected bursts of Table 2 have a temporal behaviour similar to the detected afterglows of Table 1 than the temporal optical decay at early times appears to be shallow, not steep. Another possibility could be an excess of X-ray emission at late time; if late-time central engine activity is responsible for the production of the early X-ray afterglow in some cases, the additional emission will mask the forward shock X-ray emission and the total flux in the X-ray band would be higher than the value expected for the forward shock emission alone. This might explain some dark bursts and their distribution on the Log F_O-Log F_X diagram. A combination of these mechanisms and others (i.e. intrinsic optical faintness, low density circumburst medium) may combine to explain the high number of bursts that remain undetected at optical wavelengths ($\sim 46\%$ in our sample).

5. Conclusions

- We have classified our afterglows sample into four groups based on breaks in the optical and the X-ray afterglow light curves during the decay phase. We have used the temporal and spectral properties of the X-ray and optical afterglows to investigate the blastwave physics around the break times within the framework of the standard fireball model (the synchrotron shock model). The majority of the bursts in our sample (15 out of 24) are consistent with the standard model. However, for a significant fraction of our sample (9 bursts: GRB 050713A, GRB 051111, GRB 060204B, GRB 060512, GRB 060927, GRB 061121, GRB 061126, GRB 070208 and GRB 070419A), the data cannot be explained by the standard model, even if modifications to the simple model are made (i.e. energy injection or variation in the ambient matter). A possible explanation beyond the standard model is that the early X-ray afterglow is not due to forward shock emission but is instead produced by late-time central engine activity (e.g. Ghisellini et al. 2007).

- We have derived the light curves of the optical afterglows in the source rest frame for those bursts with spectroscopically confirmed redshifts (i.e. not merely assuming a fixed redshift z=1 for all bursts). The optical luminosity function measured at $t = 10$ mins and the corresponding distributions for light curves extrapolated to $t =$ 12 hours and 1 day are uni-modal, showing no evidence for the bi-modality suggested by previous authors. A fit of the distribution at 10 minutes with a single log-normal yields an average and a sigma values of $\log L(\mathrm{erg\ s^{-1}}) = 46.55 \pm 0.18$ and $\sigma = 1.23 \pm 0.15$, respectively. Liang & Zhang (2006) reported a bimodal distribution of optical luminosity at t= 1 day. Two recent studies on the afterglows of *Swift*-era GRBs (Kann et al. 2007 and Nardini et al. 2007) also suggested a clustering of optical afterglow luminosities at one day and 12 hours (already found by Kann et al. 2006, and Nardini et al. 2006), showing again a bi-modality in the luminosity distribution. This discrepancy may be explained by our ability to detect fainter GRBs at high redshift; in future, larger samples covering a wide range of GRB luminosities (possibly facilitated by lower triggering thresholds on *Swift*) will provide stronger tests for the existence of separate classes of GRBs.

- By comparing X-ray flux densities and optical upper limits, we have shown that the majority of non-detections in our sample should be classified as dark bursts. The rapid response of our telescopes to real-time localisations from *Swift* show that there remains a significant number of genuinely dark GRB afterglows and rapid optical temporal decay at early time is ruled out as an explanation for failure to detect optical afterglows at later time. Of our 39 non-detections, ten afterglows were identified by other facilities, primarily at NIR wavelengths, demostrating a small population of bursts in high density host environments. The lack of optical/IR afterglows for the remaining 29 bursts may be due to effects such as high levels of extinction (Galactic or host), circumburst absorption, Ly-α absorption due to high-redshift or low-density environments suppressing production of optical sychrotron (or a combination of effects). Alternatively, we suggest that if late-time central engine activity is responsible for the production of the early X-ray afterglow emission in some cases, the additional emission will mask the simultaneous, but fainter forward shock X-ray emission and result in an observed X-ray flux that is larger than expected from forward shock emission alone. This might explain some dark bursts.

AM acknowledge founding from the Particle Physics and Astronomy Research Council (PPARC). CGM acknowledges financial support from the Royal Society and Research Councils UK. The Liverpool Telescope is operated by Liverpool John Moores University at

the Observatorio del Roque de los Muchachos of the Instituto de Astrofisica de Canarias. The Faulkes Telescopes, now owned by Las Cumbres Observatory, are operated with support from the Dill Faulkes Educational Trust. This research has made use of the NASA/IPAC Extragalactic Database (NED) which is operated by the Jet Propulsion Laboratory, California Institute of Technology, under contract with the National Aeronautics and Space Administration.

REFERENCES

Barthelmy S.D. et al., 2005, Space Science Reviews, 120, 143

Berger E. & Kulkarni S.R., 2005a, GCN Circ. 2978

Berger E. & Kulkarni S.R., 2005b, GCN Circ. 2983

Bloom J.S., Foley R.J., Koceveki D. & Perley D., 2006a, GCN Circ. 5217

Bloom J.S., Perley D.A. & Chen H.W., 2006b, GCN Circ. 5826

Burrows D.N. et al., 2005, Space Science Reviews, 120, 165

Burrows D.N. & Racusin J., arXiv:astro-ph/0702.633

Butler N. et al., 2005, ApJ, 629, 908

Butler N. et al., 2006, ApJ, 652, 1390

Butler N., Kocevski D., Bloom J.S. & Curtis J.L., 2007, ApJ, 671, 656

Campana S. & De Luca A., 2006, GCN Circ. 5157

Castro-Tirado A. J. et al., 2007, GCN Circ. 6168

Cenko S.B., Gezari S., Small T., Fox D.B. & Berger E., 2007, GCN Circ. 6322

Chapman R., Tanvir N.R., Priddey R.S., Levan A.J., 2007, MNRAS, 382, 21

Chen H., Thompson I., Prochaska J.X. & Josh Bloom J.S., 2005, GCN Circ. 3709

Conciatore M.L., Stratta G., Perri M., Sato G. & Burrows D., 2007, GCN Circ. 6085

Covino S., Malesani D. & Tagliaferri G., 2006, GCN Circ. 5604

Cucchiara A., Fox D.B. & Berger E., 2006, GCN Circ. 4729

Cucchiara A., Fox D.B., Cenko S.B. & Price D.A., 2007, GCN Circ. 6083

Curran P. et al., 2007, A&A, 467, 1049

D'Avanzo P. & Israel G.L., 2006a, GCN Circ. 4893

D'Avanzo P., Covino S., Malesani D. & Tagliaferri G., 2006b, GCN Circ. 5609

Dupree A.K., Falco E., Prochaska J.X., Chen H.W. & Bloom J.S., 2006, GCN Circ. 4969

Evans P.A. et al., 2007, A&A, 469, 379

Falcone A.D., Burrows D.N., Morris D.C. & Gehrels N., 2006a, GCN Circ. 4669

Falcone A. et al., 2006b, GCN Circ. 5009

Fox D.B., 2006, GCN Circ. 5605

Fox D.B., Rau A. & Ofek E.O., 2006a, GCN Circ. 5597

Fox D.B., 2006b, GCN Circ. 5607

Frail D. A. et al., 2001, ApJ, 562, L55

Fugazza D. et al., 2004, GCN Circ. 2782

Fynbo J.P.U. et al., 2006c, GCN Circ. 5809

Garnavich P., Zhao X. & Pimenova T., 2004, GCN Circ. 2792

Gehrels N. et al., 2004, ApJ, 611, 1005

Ghisellini G., Celotti A., Ghirlanda G., Firmani C. & Nava L., 2007, MNRAS, 382, L72

Godet O., Page K.L. & Burrows D.N., 2006, GCN Circ. 5128

Gomboc A. et al., 2006, Il Nuovo Cimento, 121B, 1303

Gomboc A. et al., 2008, submitted to ApJ

Graham J.F. et al., 2007, GCN Circ. 6836

Grupe D., Fox D.B., Racusin J. & Kennea J., 2006, GCN Circ. 5811

Guetta D. et al., 2007, A&A, 461, 95

Guidorzi C. et al., 2005a, GCN Circ. 3625

Guidorzi C. et al., 2005b, ApJ, 630, L121

Guidorzi C. et al., 2006, PASP, 118, 288

Guidorzi C. et al., 2007, A&A, 463, 539

Hearty F. et al., 2006a, GCN Circ. 4604

Hearty F. et al., 2006b, GCN Circ. 4611

Hill G., Prochaska J.X, Fox D.B. Schaefer B. & Reed M., 2005, GCN Circ. 4255

Hunsberger S. et al., 2005, GCN Circ. 2982

Jakobsson P. et al., 2004, ApJ, 617, L21

Jakobsson P. et al., 2006, A&A, 447, 897

Jakobsson P. et al., 2007, GCN Circ. 6283

Jensen B.L., Hjorth J., Fynbo J. & Näränen J., 2006, GCN Circ. 5203

Kann D.A., Klose S. & Zeh A., 2006, ApJ, 641, 993

Kann D.A. et al., 2007, astro-ph/0712.2186

Kobayashi S. & Zhang B., 2003, ApJ, 582, L75

Kobayashi S. & Zhang B., 2007, ApJ, 655, 973

Kocevski D., Bloom J.S. & McGrath E.J., 2006a, GCN Circ. 4528

Kocevski D., Bloom J.S. & McGrath E.J., 2006b, GCN Circ. 4540

Le T. & Dermer C. D., 2007, ApJ, 661, 394

Levan A.J. et al., 2006, ApJ, 648, L9

Liang E. & Zhang B., 2006, ApJ, 638, L67

Liang E., Zhang B., Virgili F. & Dai Z.G., 2007, ApJ, 662, 1111

Lin Z.Y. et al., 2005, GCN Circ. 2976

Lipunov V. et al., 2006, GCN Circ. 4892

Malesani D. et al., 2004, ApJ, 609, L5

Malesani D. et al., 2006a, GCN Circ. 4541

Malesani D. et al., 2006b, GCN Circ. 4561

Malesani D. et al., 2006c, GCN Circ. 5705

Malesani D. et al., 2006d, GCN Circ. 5718

Mészáros P. & Rees M.J., 1999, MNRAS, 306, L39

Mészáros P., 2002, ARA&A, 40, 137

Molinari E. et al., 2007, A&A, 469, L13

Monfardini A. et al., 2006, ApJ, 648, 1125

Moretti A., Romano P. & Guidorzi C., 2007, GCN Circ. 6286

Morris D.C., Burrows D.N., Gehrels N., Boyd P. & Voges W., 2006a, GCN Circ. 4651

Morris D.C., Pagani C., Burrows D.N., Kennea J.A. & Page K.L., 2006b, GCN Circ. 4764

Morris D.C. et al., 2007, ApJ, 654, 413

Mundell C. et al., 2007a, Science, 315, 1822

Mundell C. et al., 2007b, ApJ, 660, 489

Nardini M. et al., 2006, A&A, 451, 821

Nardini M., Ghisellini G. & Ghirlanda G., 2007, astro-ph/0801.4759

Nousek J.A. et al., 2006, ApJ, 642, 389

O'Brien, P.T. et al., 2006, ApJ, 647 1213

Oates S. et al., 2006, MNRAS, 372, 327

Osip D., Chen H.W. & Prochaska J.X., 2007, GCN Circ. 5715

Page K.L. et al., 2007, ApJ, 663, 1125

Panaitescu A. & Kumar P., 2001, ApJ, 560, L49

Panaitescu A. et al., 2006, MNRAS, 369, 2059

Pandey S.B. et al., 2006, A&A, 460, 415

Perri M. et al., 2006, GCN Circ. 5110

Perri M. et al., 2007, GCN Circ. 6333

Perley D.A. et al., 2007, astro-ph/0703.538

Piran T., 1999, Physics Reports, 314, 575

Price P.A., 2006, GCN Circ. 5104

Prochaska J.X., Ellison S., Foley R.J., Bloom J.S. & Chen H.W., 2005, GCN Circ. 3332

Prochaska J.X. et al., 2006, GCN Circ. 4701

Racusin J., Kennea J., Pagani C., Vetere L. & Evans P., 2007, GCN Circ. 6627

Rees M.J. & Mészáros P., 1992, MNRAS, 258, 41

Rol E. et al., 2007, GCN Circ. 6221

Rol E. et al., 2007b, MNRAS, 374, 1078

Ruiz-Velasco A.E. et al., 2007, ApJ, 669, 1

Sari R., Piran T. & Narayan R., 1998, ApJ, 497, L17

Sari R., Piran T. & Halpern J.P., 1999, ApJ, 519, L17

Sari R. & Piran T., 1999, ApJ, 520, 641

Schady P. et al., 2007, MNRAS, 380, 1041

Schlegel D. et al., 1998, ApJ, 500, 525

Smith J.A. et al., 2002, AJ, 123, 2121

Soderberg A.M. et al., 2006, ApJ, 636, 391

Stanek K.Z. et al., 2003, ApJ, 591, L17

Stanek K.Z. et al., 2005, ApJ, 626, L5

Stratta G., Perri M., Burrows D.N. & Stamatikos M., 2007, GCN Circ. 6337

Swan H., Akerlof C., Rykoff E., Yost S. & Smith I., 2006, GCN Circ. 4568

Tagliaferri G. et al., 2005, Nature, 436, 985

Tanvir N.R. et al., 2005, GCN Circ. 3632

Tanvir N.R., Levan A.J., Priddey R.S., Fruchter A.S. & Hjorth J., 2006a, GCN Circ. 4602

Tanvir N.R., Rol E., Wiersema K., Starling R. & O'Mahoney N., 2006b, GCN Circ. 4897

Tanvir N.R. et al., 2008, astro-ph/0803.4100

Yost S.A. et al., 2006, ApJ, 636, 959

Yost S.A. et al., 2007, ApJ, 657, 925

Willingale, R. et al., 2007, ApJ, 662, 1093

Woosley S.E. & Bloom J.S., 2006, ARA&A, 44, 507

Wreeswijk P. & Jaunsen A., 2006, GCN Circ. 4974

Zhang B., Kobayashi S. & Mészáros P., 2003, ApJ, 595, 950

Zhang B. et al., 2006, ApJ, 642, 354

This preprint was prepared with the AAS LaTeX macros v5.2.

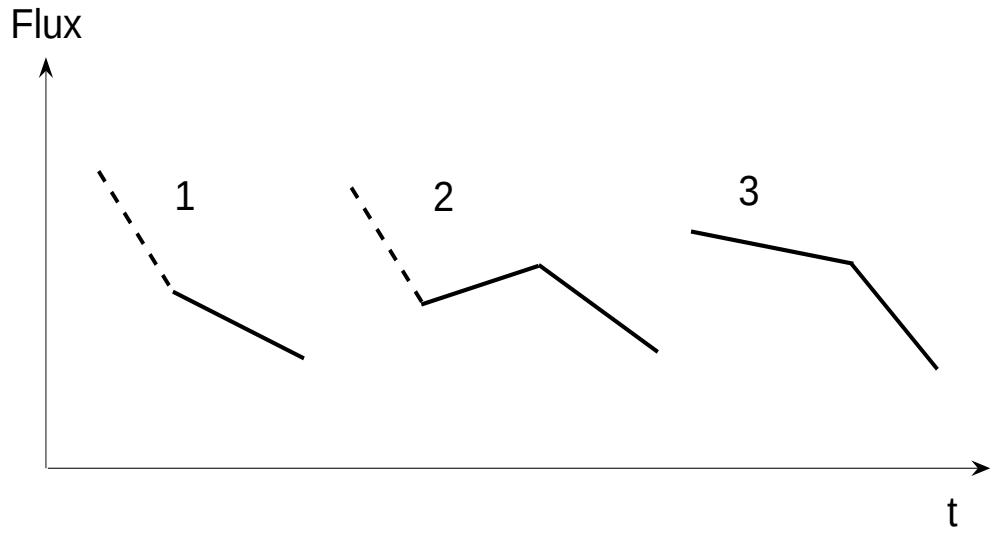

Fig. 1.— Schematic illustrating possible shapes of the optical light curves at early times as a result of the contribution of reverse and forward shock emissions (case 1 and 2) or due to energy injection (case 3). The thick dashed line for case 1 and 2 represent the reverse shock contribution at early times, that can be missing if the observations do not start early enough.

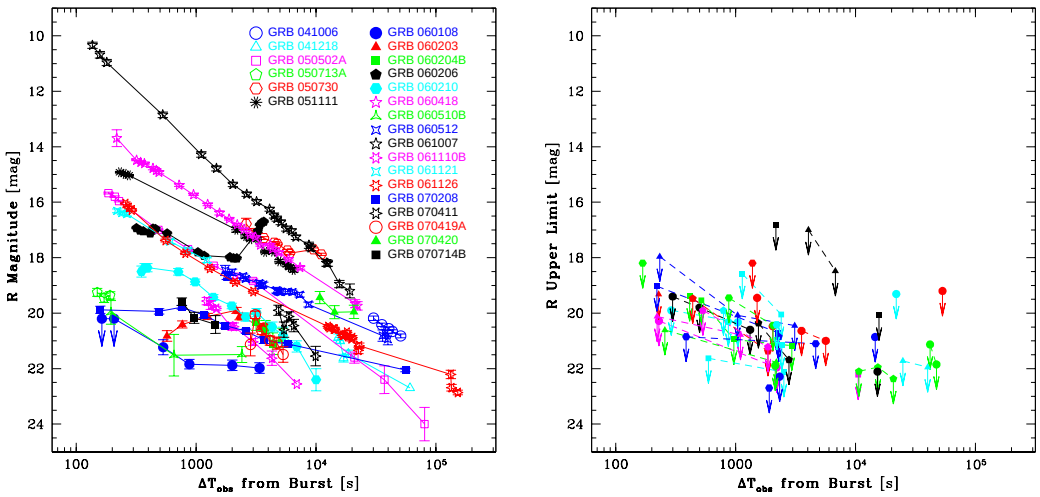

Fig. 2.— Left panel: observed light curves in the R filter of all the detected afterglows in our sample. GRB 060927 is not included as we detected this burst only in the i' band (see Ruiz-Velasco et al. 2007). Right panel : optical upper limits in the R band of the remaining GRBs observed with, but not detected by the Liverpool and Faulkes telescopes. Connected symbols refer to different observations for the same burst when additional late time observations were available.

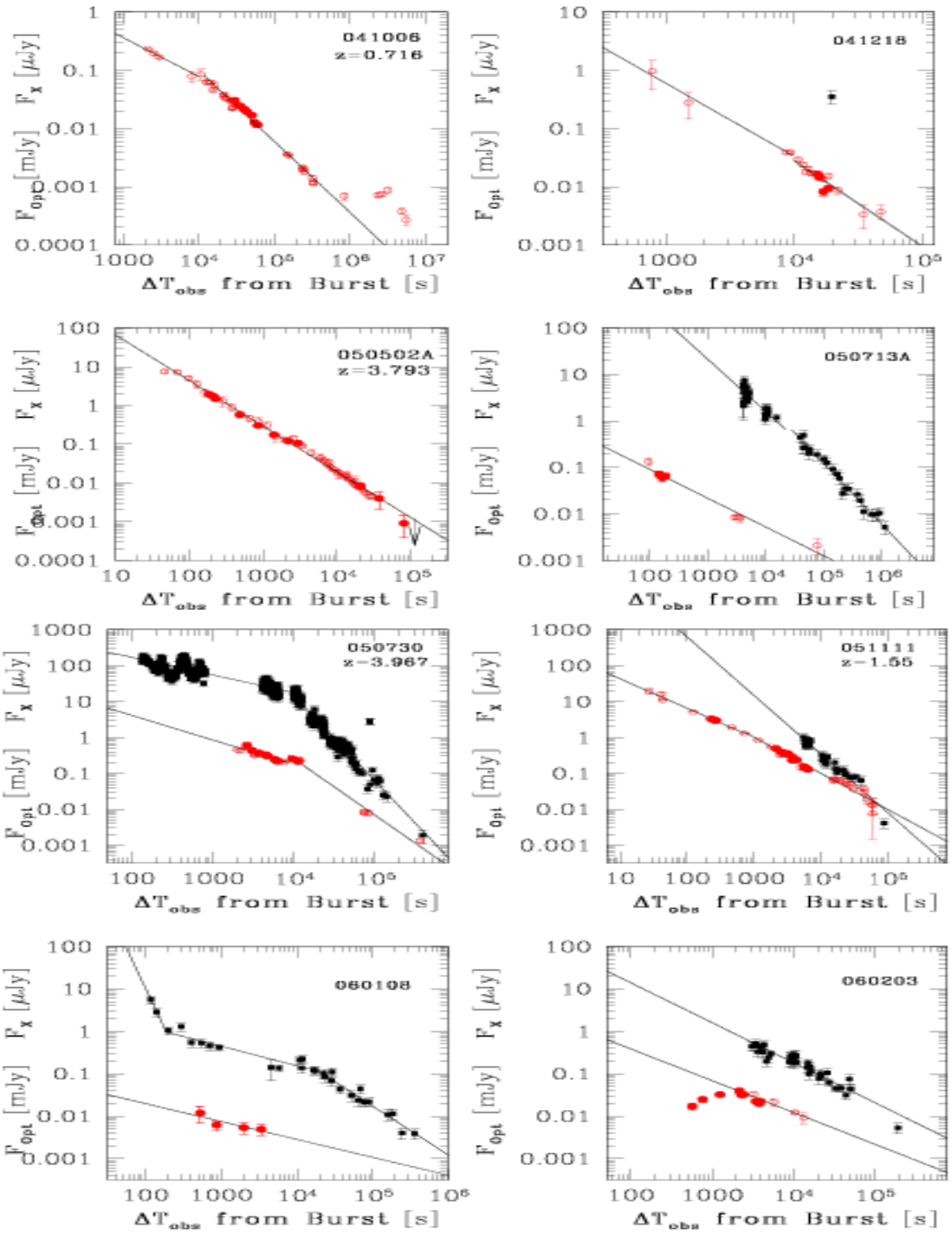

Fig. 3.— X-ray and optical (R-band) light curves for the 24 GRB afterglows detected by our telescopes from October 2004 to September 2007. For each burst we show the X-ray flux density in μJy (black filled squares) and optical flux density in mJy (red filled circles for our observations and red open circles for published data, when available). We show also the value of the spectroscopic redshift when available. X-ray data of *Swift*/XRT are from Evans et al. (2007). We superimpose simple power-law fit segments to each curve (the details of the fit are reported on Table 1).

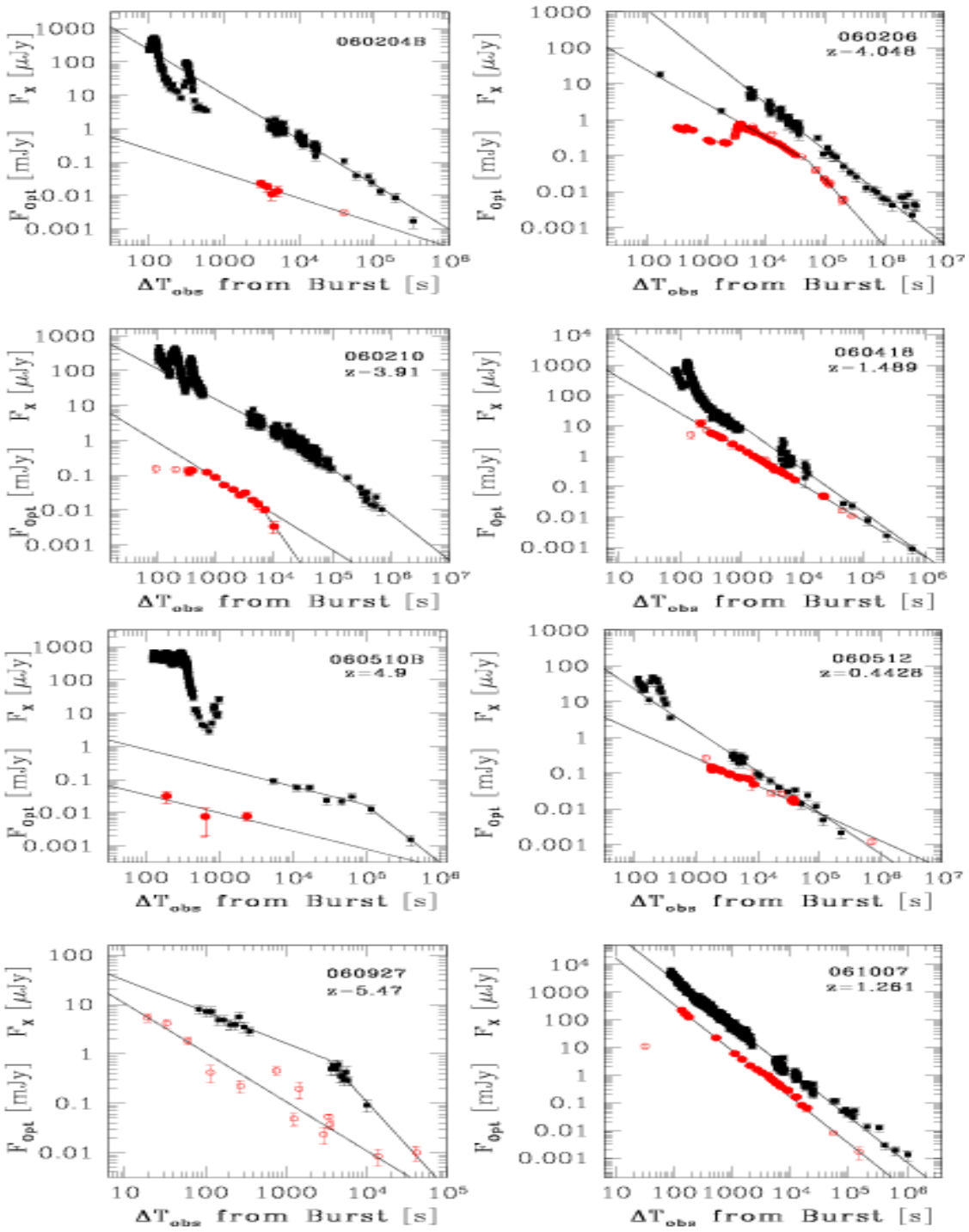

Fig. 3.— - continued. For GRB 060927 there are no data in the R band because we detected this burst only in the i' filter due to its high redshift ($z = 5.467$).

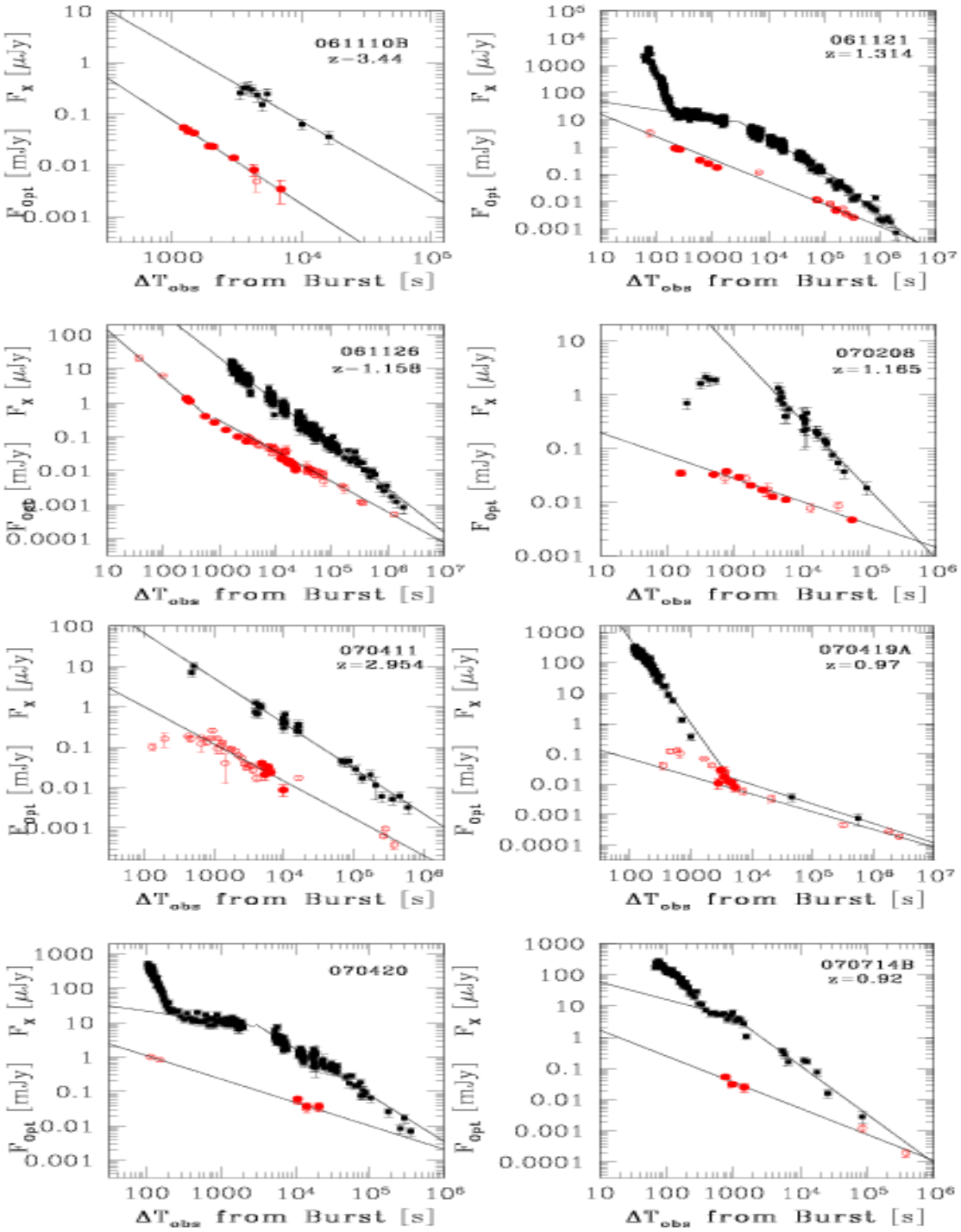

Fig. 3.— - continued.

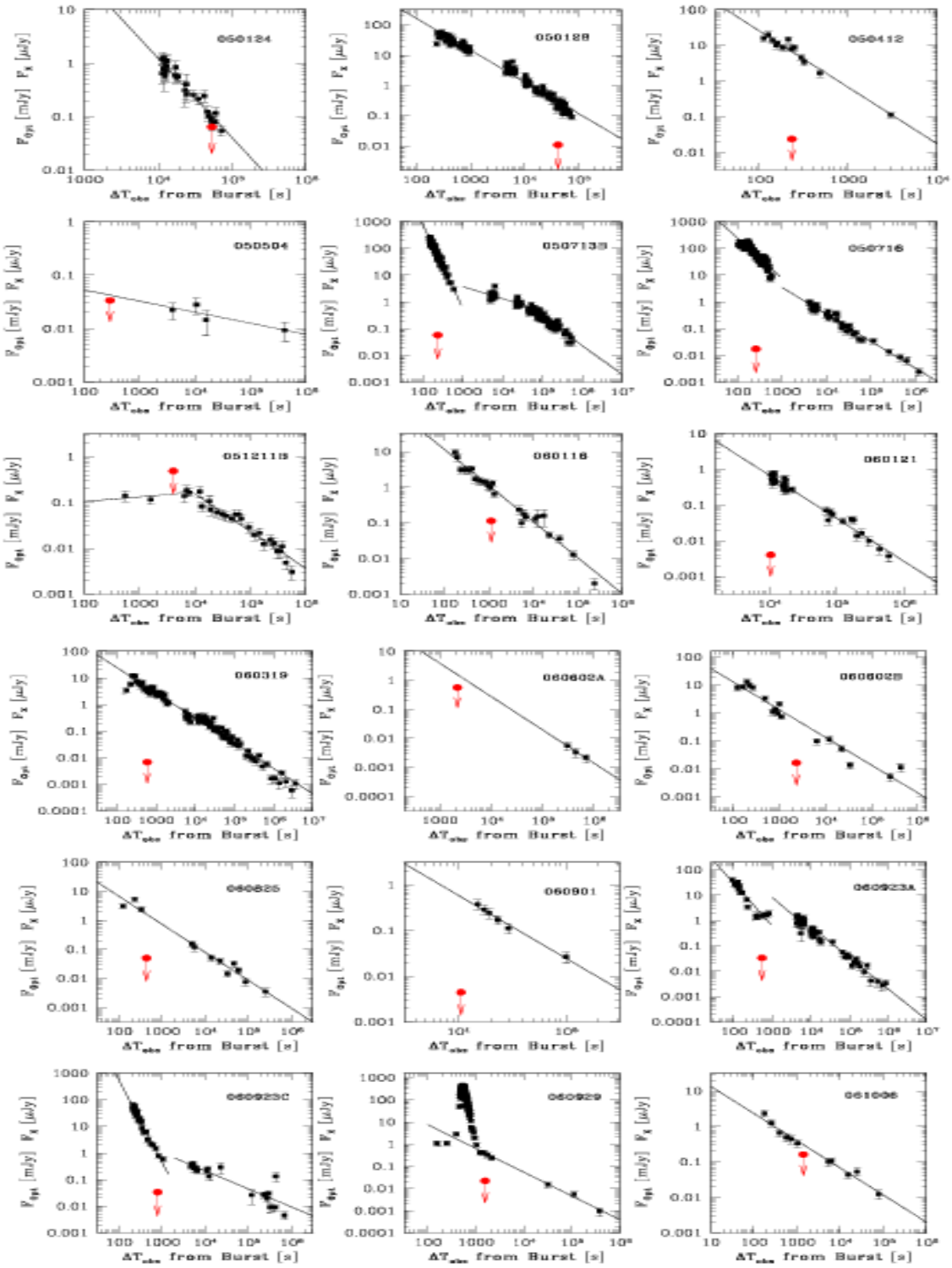

Fig. 4.— X-ray light curves (black squares) for some GRBs for which we provide deep optical upper limit (red dots). These are the bursts in Table 2 that have been observed by the *Swift*-XRT (data from Evans et al. 2007).

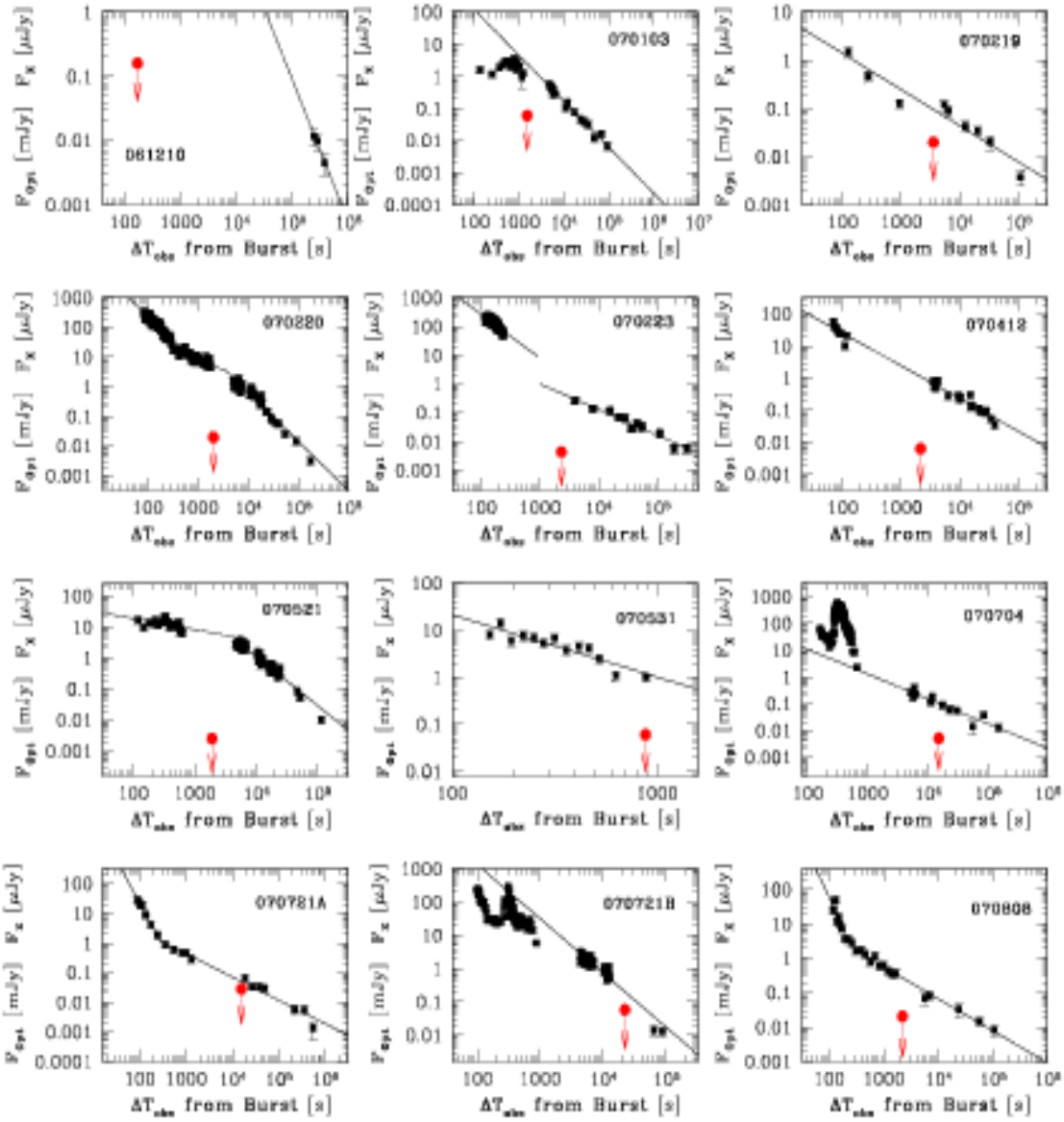

Fig. 4.— - continued.

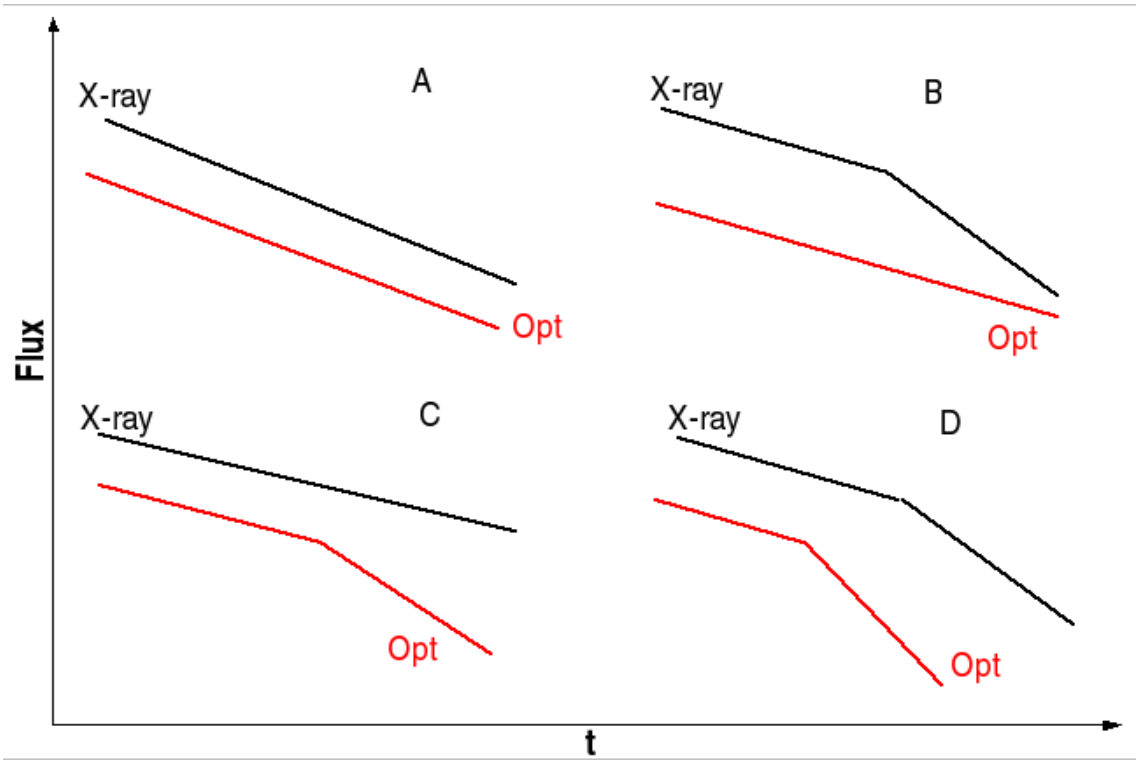

Fig. 5.— Schematic view of the observed shapes of light curves in the optical (red) and X-ray band (black).

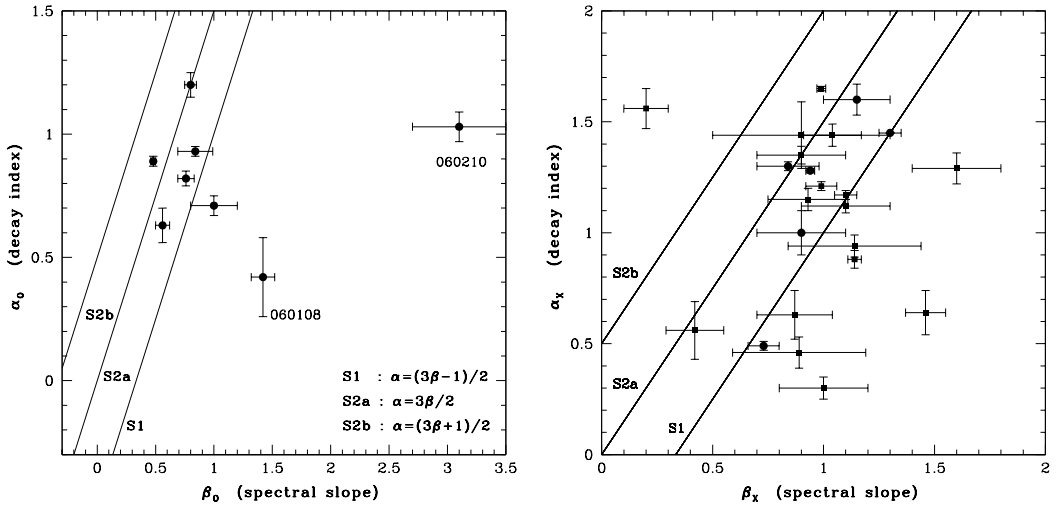

Fig. 6.— Left panel : optical spectral slope ($\beta_{\rm O}$) vs optical temporal decay index ($\alpha_{\rm O}$). Right panel : spectral slope ($\beta_{\rm X}$) vs temporal decay ($\alpha_{\rm X}$) in the X-ray band. The three lines drawn are the closure relations expected for the standard fireball model: S1 = spherical outflow with the cooling frequency ($\nu_{\rm c}$) below the observing frequency (optical or X-ray), S2a = spherical outflow with $\nu_{\rm c}$ above the observing frequency in a homogeneous medium, S2b = spherical outflow with $\nu_{\rm c}$ above the observing frequency in a wind-like medium.

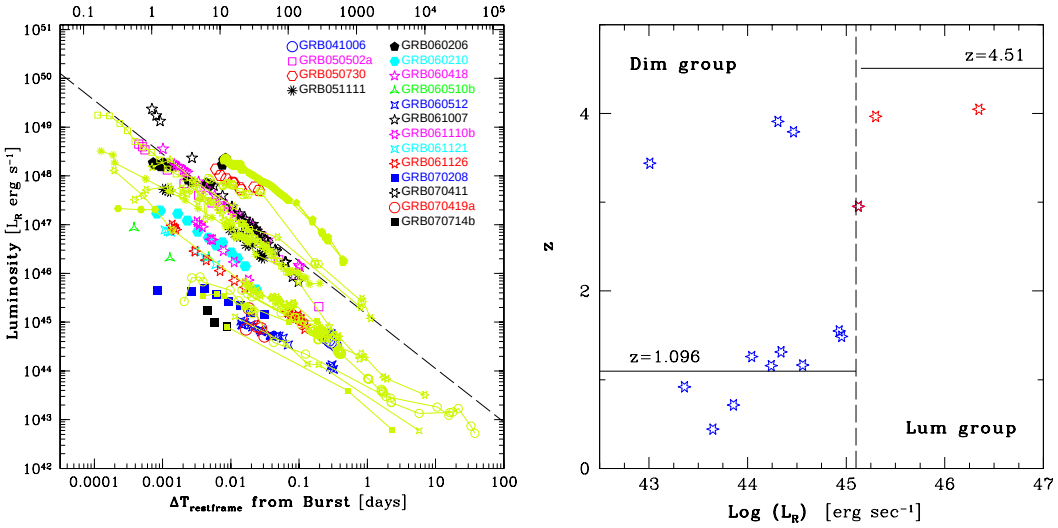

Fig. 7.— Left panel: rest frame luminosity for all the afterglows in our sample with known spectroscopic redshift. We superimposed on our data all the published data (GCNs and refereed journal papers). The time axis is given in days for an easier comparison with the similar plot of LZ06 and the same time in the restframe $\Delta T_{\rm rest-frame}$ is given along the top of the plot in seconds to be consistent with the earlier plots. The black dotted line shows the luminosity separation (L_*) between luminous and dim bursts as defined by LZ06, see text for details. Right panel: luminosity rest frame at 1 day against redshift for the bursts of our sample. The vertical line is L_* and the two horizontal lines show the biggest values for the redshift of the two classes of LZ06.

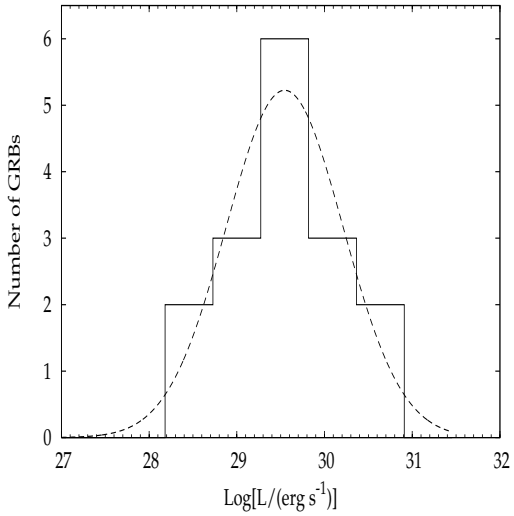

Fig. 8.— The observed luminosity distribution of our sample at 12 hours, fitted with a single log-normal function with an average of 29.54 ± 0.07 and a σ of 0.67 ± 0.05.

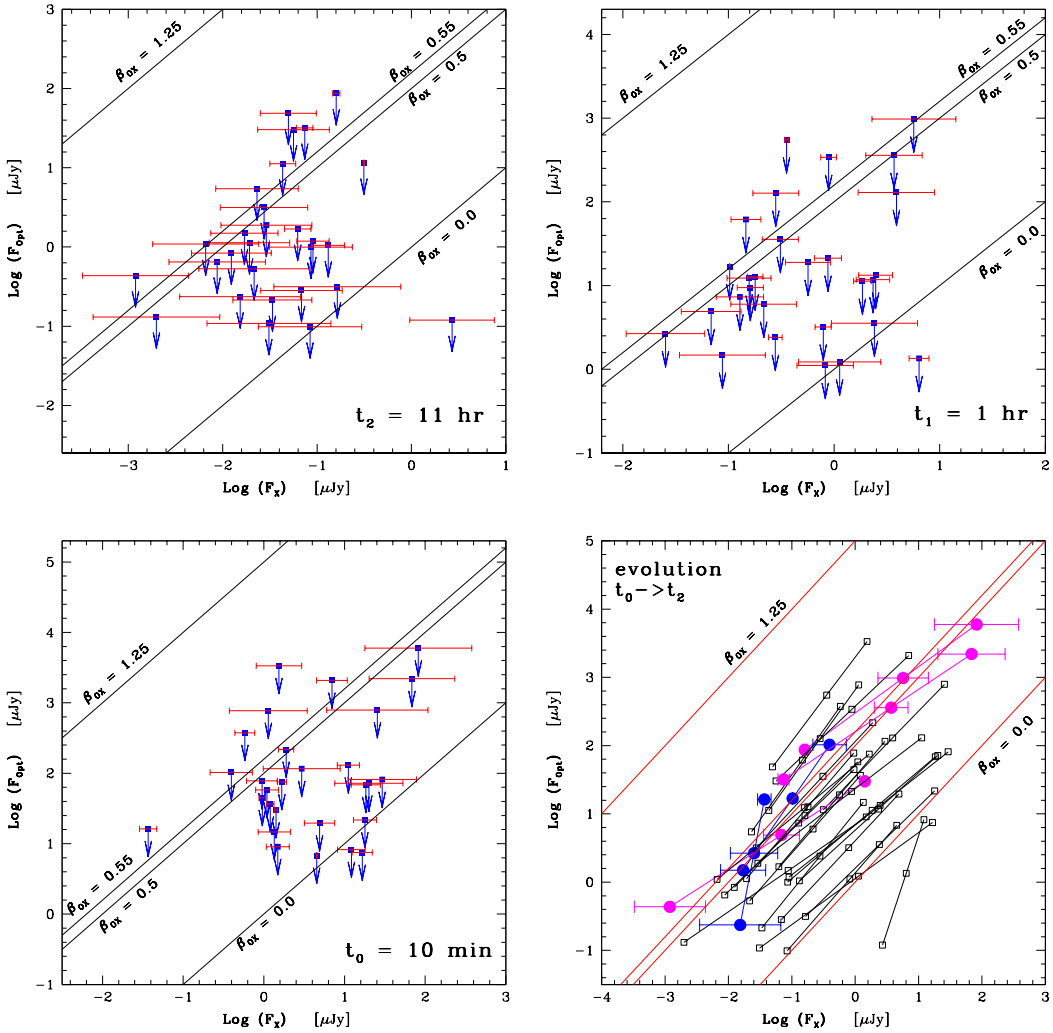

Fig. 9.— Plots of optical flux ($F_{\rm O}$) versus X-ray flux ($F_{\rm X}$) for all the bursts listed in Table 2 for which an XRT observation was available. Extrapolation of the fluxes has been done at t_2=11 hours (top left), t_1=1 hour (top right) and t_0=10 minutes (bottom left). Lines with constant $\beta_{\rm OX}$ are shown. Dark bursts are the ones below the constant line $\beta_{\rm OX} = 0.5$. The plot at bottom right shows the evolution of the optical and X-ray flux from t_0 to t_2; for clarity the errors on this panel are not shown.

Table 1. Optical and X-ray light curves parameters. If data are well fitted with a broken power law then α_1 and α_2 represent the decay index pre- and post-break respectively and $t_{\rm break}$ is the break time, for both optical and X-ray bands. The value of the reduced χ^2 (χ^2/ν, where ν are the degrees of freedom) is given for each fit in the two bands. The values of $\beta_{\rm O}$, $\beta_{\rm X}$ and $\beta_{\rm OX}$ are the slopes of the spectral energy distribution taken from the literature. In the last two columns we report the value of the redshift (z) and the isotropic energy ($E_{\gamma,\rm iso}$) of the burst when available. * = this value refers to R band data taken from GCNs because we detected GRB 060927 only in the i' band, due to the high redshift of the event.

GRB	$\alpha_{\rm O,1}$	$\alpha_{\rm O,2}$	$t_{{\rm O},break}$ (days)	χ^2/ν	$\alpha_{\rm X,1}$	$\alpha_{\rm X,2}$	$t_{{\rm X},break}$ (days)	χ^2/ν	β_O	β_X	β_{OX}	z	$E_{\gamma,\rm iso}$ [10^{52} erg]
041006	0.71 ± 0.04	1.24 ± 0.01	0.15 ± 0.01	77/72	—	1.0 ± 0.1	—	—	1.0 ± 0.2	0.9 ± 0.2	~ 0.7	0.716	$0.94^{+0.21}_{-0.08}$
041218	1.25 ± 0.10	1.47 ± 0.13	0.11 ± 0.01	19/16	—	—	—	—	—	—	—	—	—
050502A	1.20 ± 0.04	—	—	50/52	> 1.45	—	—	—	0.80 ± 0.05	1.30 ± 0.05	0.8 ± 0.1	3.793	4^{+3}_{-1}
050713A	0.63 ± 0.04	—	—	12/6	1.17 ± 0.05	1.32 ± 0.09	0.28 ± 0.06	53/45	—	1.10 ± 0.05	1.2 ± 0.1	—	—
050730	0.63 ± 0.07	1.55 ± 0.08	0.10 ± 0.01	46/45	0.49 ± 0.02	2.37 ± 0.05	0.11 ± 0.01	670/566	0.56 ± 0.06	0.73 ± 0.07	—	3.967	9^{+8}_{-3}
051111	0.82 ± 0.03	1.00 ± 0.03	0.008 ± 0.001	46/43	—	1.60 ± 0.07	—	34/29	0.76 ± 0.07	1.15 ± 0.15	0.84 ± 0.02	1.55	6^{+5}_{-2}
060108	0.42 ± 0.16	—	—	5/4	0.46 ± 0.07	1.15 ± 0.07	0.18 ± 0.02	29/25	~ 1.4	0.89 ± 0.30	0.54 ± 0.10	< 3.2	< 0.795
060203	0.74 ± 0.13	—	—	11/8	0.94 ± 0.05	—	—	41/34	—	1.24 ± 0.30	—	—	—
060204B	0.73 ± 0.10	—	—	4/3	—	1.35 ± 0.04	—	54/60	—	0.9 ± 0.2	—	—	—
060206	0.93 ± 0.02	1.83 ± 0.02	0.60 ± 0.01	235/216	1.30 ± 0.02	—	—	66/72	0.84 ± 0.15	0.84 ± 0.14	0.93 ± 0.02	4.048	$4.1^{+1.2}_{-0.6}$
060210	1.03 ± 0.06	(2.38 ± 0.43)	(0.10 ± 0.02)	9/7	0.88 ± 0.04	1.31 ± 0.03	0.33 ± 0.03	263/221	3.1 ± 0.4	1.14 ± 0.03	0.3 ± 0.1	3.91	42^{+35}_{-8}
060418	1.19 ± 0.02	—	—	29/26	1.44 ± 0.05	—	—	97/80	—	1.04 ± 0.13	—	1.489	10^{+7}_{-2}
060510B	0.55 ± 0.34	—	—	2/1	0.56 ± 0.13	1.7 ± 0.1	1.16 ± 0.02	5/6	—	0.42 ± 0.13	—	4.9	23^{+10}_{-4}
060512	0.77 ± 0.02	—	—	19/22	1.15 ± 0.05	—	—	22/17	—	0.93 ± 0.18	—	0.4428	$0.020^{+0.030}_{-0.004}$
060927	$0.99 \pm 0.11^*$	—	—	19/11	0.63 ± 0.11	1.78 ± 0.21	0.035 ± 0.003	16/13	—	0.87 ± 0.17	—	5.467	9^{+2}_{-1} |
061007	1.71 ± 0.02	—	—	24/23	1.65 ± 0.01	—	—	954/978	—	0.99 ± 0.02	1.02 ± 0.05	1.261	140^{+110}_{-60}
061110B	1.64 ± 0.08	—	—	8/7	1.44 ± 0.15	—	—	11/7	—	0.9 ± 0.4	—	3.44	13^{+16}_{-6}
061121	0.83 ± 0.03	—	—	41/36	1.21 ± 0.02	1.58 ± 0.12	2.89 ± 0.03	200/191	—-	0.99 ± 0.07	0.53 ± 0.06	1.314	19^{+11}_{-5} |
061126	1.43 ± 0.12	0.89 ± 0.02	0.009 ± 0.001	93/72	—	1.28 ± 0.01	—	348/273	0.48 ± 0.02	0.98 ± 0.02	0.53 ± 0.02	1.158	8^{+7}_{-2}
070208	0.42 ± 0.04	—	—	14/11	—	1.29 ± 0.07	—	36/24	—	1.6 ± 0.2	—	1.165	$0.28^{+0.22}_{-0.08}$
070411	0.92 ± 0.04	—	—	61/38	1.12 ± 0.03	—	—	39/28	—	1.1 ± 0.2	—	2.954	10^{+8}_{-2}
070419A	—	0.58 ± 0.04	—	21/9	2.79 ± 0.06	0.64 ± 0.10	0.046 ± 0.005	139/105	—	1.46 ± 0.09	—	0.97	$0.24^{+0.23}_{-0.03}$
070420	0.68 ± 0.03	—	—	4/3	0.30 ± 0.05	1.34 ± 0.03	0.034 ± 0.04	232/142	—	1.0 ± 0.2	—	—	—
070714B	0.83 ± 0.04	—	—	5/3	0.56 ± 0.19	1.56 ± 0.09	0.010 ± 0.02	28/19	—	0.2 ± 0.1	—	0.92	$0.8^{+2.0}_{-0.1}$

Note. — Notes - References for $\alpha_{\rm X,1}$: GRB 050502A : (Guidorzi et al. 2005b). References for $\alpha_{\rm X,2}$: GRB 041006 : (Butler et al. 2005). References for $\beta_{\rm O}$: GRB 041006 : (Garnavich et al. 2004); GRB 050502A : (Guidorzi et al. 2005b; Yost et al. 2006); GRB 050730 : (Pandey et al. 2006); GRB 051111 : (Guidorzi et al. 2007); GRB 060108 : (Oates et al. 2006); GRB 060206 : (Monfardini et al. 2006); GRB 060210 : (Curran et al. 2007); GRB 061126 : (Gomboc et al. 2008). References for $\beta_{\rm X}$: GRB 041006 : (Butler et al. 2005); GRB 050502A : (Guidorzi et al. 2005b); GRB 050713A : (Morris et al. 2007); GRB 050730 : (Pandey et al. 2006); GRB 051111 : (Guidorzi et al. 2007); GRB 060108 : (Oates et al. 2006); GRB 060203 : (Morris et al. 2006a); GRB 060204B : (Falcone et al. 2006a); GRB 060206 : (Monfardini et al. 2006); GRB 060210 : (Curran et al. 2007); GRB 060418 : (Falcone et al. 2006b); GRB 060510B : (Perri et al. 2006); GRB 060512 : (Godet et al. 2006); GRB 060927 : (Ruiz-Velasco et al. 2007); GRB 061007 : (Schady et al. 2006); GRB 061110B : (Grupe et al. 2006); GRB 061121 : (Page et al. 2007); GRB 061126 : (Gomboc et al. 2008); GRB 070208 : (Conciatore et al. 2007); GRB 070411 : (Moretti et al. 2007); GRB 070419A : (Perri et al. 2007); GRB 070420 : (Stratta et al. 2007); GRB 070714B : (Racusin et al. 2007). References for $\beta_{\rm OX}$: GRB 041006 : (Butler et al. 2005). GRB 050502A : (Guidorzi et al. 2005b); GRB 050713A : (Morris et al. 2007); GRB 051111 : (Guidorzi et al. 2007); GRB 060108 : (Oates et al. 2006); GRB 060206 : (Monfardini et al. 2006); GRB 060210 : (Curran et al. 2007); GRB 061007 : (Mundell et al. 2007b); GRB 061121 : (Page et al. 2007); GRB 061126 : (Gomboc et al. 2008). References for z : GRB 041006 : (Fugazza et al. 2004); GRB 050502A : (Prochaska et al. 2005); GRB 050730 : (Chen et al. 2005); GRB 051111 : (Hill et al. 2005); GRB 060108 : (Oates et al. 2006); GRB 060206 : (Prochaska et al. 2006); GRB 060210 : (Cucchiara et al. 2006); GRB 060418 : (Dupree et al. 2006; Wreeswjk & Jaunsen 2006); GRB 060510B : (Price et al. 2006); GRB 060512 : (Bloom et al. 2006a); GRB 060927 : (Ruiz-Velasco et al. 2007); GRB 061007 : (Osip et al. 2007); GRB 061110B : (Fynbo et al. 2006); GRB 061121 : (Bloom et al. 2006b); GRB 061126 : (Perley et al. 2007); GRB 070208 : (Cucchiara et al. 2007); GRB 070411 : (Jakobsson et al. 2007); GRB 070419A : (Cenko et al. 2007); GRB 070714B : (Graham et al. 2007). References for $E_{\gamma,\rm iso}$: (all values from Butler et al. 2007, except for GRB 041006, GRB 050502A and GRB 060108).

Table 2. Upper limit parameters. Refer to Section 3.2 for detailed explanation of the colums of that table.

GRB	XRT pos.	Duration (s)	f $\times 10^7$ (erg cm^{-2})	F_X $\times 10^{11}$ (erg cm^{-2} s^{-1})	$\Delta\ t_X$ (min)	α_X	β_X	$\Delta\ t_{start}$ (min)	$R^{u.l.}_{start}$	$\Delta\ t_{mean}$ (min)	$R^{u.l.}_{mean}$	T_{exp} (min)	OT	A_R	$\alpha_X^{(fit)}$	F_X ($\Delta\ t_R$) (μ Jy)
041211	no	30.2	100	—	—	—	—	197.20	19.18	242.94	20.86	4.5	—	0.45	—	—
050124	yes	4.1	12.3	6.9	185.2	—	0.3	885.64	19.00	886.02	19.20	0.5	IR	0.09	1.49 ± 0.08	0.103
050128	yes	13.8	51.7	24.0	3.62	—	—	697.20	21.13	788.4	21.85	20.0	—	0.21	1.05 ± 0.02	0.296
050412	yes	26.0	5.66	0.39	166.7	1.35	0.4	2.5	18.7	3.83	20.82	11.5	—	0.05	1.58 ± 0.09	6.790
050504	yes	80.0	15.0	—	326.8	—	—	3.7	19.00	17.39	20.33	17.67	—	0.03	0.21 ± 0.08	0.043
050520	yes	80.0	24.0	0.01	127.7	1.4	—	4.5	16.60	8.34	19.4	2.5	—	0.04	—	—
050528	no	10.8	4.40	—	849.0	—	—	2.5	17.2	3.88	17.96	1.0	—	0.43	—	—
050713B	yes	75.0	45.7	90.2	2.27	2.88	0.7	3.3	18.2	3.80	19.32	0.5	—	1.25	3.08 ± 0.07	52.947
050716	yes	69.0	63.2	70.2	3.83	1.68	0.32	3.8	19.8	4.29	20.61	8.5	IR	0.29	1.50 ± 0.05	58.970
050925	no	0.068	0.75	—	1.66	—	—	3.3	19.0	3.69	21.12	2.0	—	5.69	—	—
051211A	no	4.2	9.2	—	—	—	—	353.4	20.86	413.4	21.72	60.5	—	0.32	—	—
051211B	yes	80.0	20.0	0.13	179.7	1.16	1.0	66.1	16.5	67.4	17.0	1.0	—	1.26	0.82 ± 0.06	0.322
060114	no	100.0	13.0	—	—	—	—	2.2	19.0	37.59	20.70	15.5	—	0.09	—	—
060116	yes	113.0	26.0	0.9	2.57	0.95	1.1	18.72	18.58	39.98	20.0	8.5	IR	0.69	1.01 ± 0.04	0.990
060121	yes	2.0	43.0	0.46	176.70	1.08	1.07	50.23	19.5	175.56	22.22	20.83	O	0.04	1.20 ± 0.04	0.644
060204C	no	60.0	3.5	0.001	2.6	—	—	6.42	18.7	6.89	19.39	1.0	—	0.49	—	—
060319	yes	12.0	2.7	2.2	2.88	1.02	1.10	7.0	19.0	9.90	21.63	3.0	IR	0.06	0.95 ± 0.02	4.559
060602A	yes	60.0	16.0	—	—	—	—	7.72	15.0	36.08	16.83	21.0	O	0.07	1.15 ± 0.13	1.595
060602B	yes	9.0	1.8	0.32	1.38	1.05	2.1	19.2	18.0	38.20	20.85	2.5	—	95.63	—	—
060825	yes	8.1	9.8	3.57	1.1	0.87	0.64	4.43	18.7	7.31	19.47	3.0	—	1.55	0.96 ± 0.05	1.626
060901	yes	20.0	7.0	0.26	226.0	1.7	1.1	142.8	21.0	177.6	22.10	20.0	—	1.85	1.38 ± 0.08	0.553
060923A	yes	51.7	8.7	4.9	1.35	2.7	1.1	2.8	19.0	8.88	19.90	2.0	IR	0.16	1.69 ± 015	1.732
060923C	yes	76.0	16.0	85.0	3.38	3.4	0.85	4.22	19.0	14.50	20.3	3.67	IR	0.17	3.09 ± 0.09	0.700
060929	yes	12.4	2.8	0.53	1.53	0.79	1.3	21.13	19.0	25.88	20.36	3.0	—	0.13	1.07 ± 0.04	0.396
060930	no	20.0	2.5	—	—	—	—	1.98	19.5	6.45	20.85	1.5	—	0.22	—	—
061006	yes	0.5	14.3	0.19	2.38	2.26	0.7	22.61	18.0	23.05	18.20	0.5	O	0.85	0.77 ± 0.04	0.306
061210	yes	0.2	11.0	—	—	—	—	2.39	17.0	2.8	18.20	0.5	—	0.09	2.20 ± 0.42	118664.2
070103	yes	19.0	3.4	0.38	1.15	1.4	1.3	23.7	19.0	25.20	19.45	1.0	—	0.18	1.42 ± 0.05	3.00
070219	yes	17.0	3.2	0.12	1.37	2.2	1.0	51.4	19.9	59.09	20.64	5.0	—	0.09	0.75 ± 0.28	0.104
070220	yes	129.0	106.0	16.5	1.32	1.76	0.55	1.93	19.5	34.01	20.47	10.0	—	2.41	0.76 ± 0.09	3.834
070223	yes	89.0	17.0	92.0	1.83	2.3	0.7	18.7	21.4	38.84	22.29	13.0	IR	0.04	0.88 ± 0.06	0.407
070412	yes	34.0	4.8	33.0	1.02	0.98	1.2	14.1	21.0	35.68	21.89	13.0	—	0.06	1.02 ± 0.03	1.34
070521	yes	37.9	80.0	3.2	1.28	0.5	1.11	2.35	19.3	31.77	22.70	12.0	—	0.07	0.36 ± 0.16	8.02
070531	yes	44.0	11.0	—	2.13	—	—	11.9	18.2	14.64	19.45	3.0	—	1.00	1.32 ± 0.17	1.01
070704	yes	380.0	59.0	285.0	2.55	0.87	0.85	239.5	21.1	254.34	22.11	30.0	—	5.01	0.92 ± 0.10	0.150
070721A	yes	3.4	0.71	0.823	1.43	2.97	1.24	229.2	19.0	261.72	20.08	15.5	—	0.04	0.78 ± 0.04	0.089
070721B	yes	340.0	36.0	24.5	1.53	0.9	0.48	327.0	18.5	364.44	19.31	15.17	—	0.08	1.63 ± 0.07	0.195
070808	yes	32.0	12.0	1.0	1.9	3.5	1.8	2.35	19.7	36.69	20.42	16.0	—	0.06	0.93 ± 0.03	0.283
070810B	yes	80.0	0.12	—	1.03	—	—	2.80	20.0	40.63	21.15	14.0	—	0.14	—	—

Note. — Notes - Reference for Duration, f, F_X, $\Delta\ t_X$, α_X and β_X : http://heasarc.gsfc.nasa.gov/docs/swift/archive/grb_table/. References for OT : GRB 050124 : (Berger et al. 2005a; Berger et al. 2005b); GRB 050716 : (Tanvir et al. 2005; Rol et al. 2007b); GRB 060116 : (Kocevski et al. 2006a; Kocevski et al. 2006b; Swan et al. 2006; Malesani et al. 2006a; Tanvir et al. 2006a); GRB060121: (Levan et al. 2006; Malesani et al. 2006b; Hearty et al. 2006a; Hearty et al. 2006b); GRB 060319 : (Tanvir et al. 2006b); GRB 060602A : (Jensen et al. 2006); GRB 060923A : (Tanvir et al. 2008; Fox et al. 2006a; Fox 2006); GRB 060923C: (Covino et al. 2006; D'Avanzo et al. 2006b); GRB 061006 : (Malesani et al. 2006c; Malesani et al. 2006d); GRB 070223 : (Castro-Tirado et al. 2007; Rol et al. 2007). Reference for A_R : the values of A_R come from the NED extinction calculator and are calculated from the list of $A_\lambda/E(B-V)$ reported in Table 6 of Schlegel et al. (1998) assuming an average value $R_V = A_V/E(B-V) = 3.1$.

Table 3. Temporal decay index α and spectral index β in the slow cooling regime as functions of the electron spectral index p for ISM (ρ=constant) or wind-like ambient medium ($\rho = R^{-2}$). The cases of energy injection ($L \propto t^{-q}$) and no energy injection (q=1) are considered (e.g. Zhang et al. 2006).

Slow cooling	β	α (no injection)	α (injection)
$\nu_{\rm m} < \nu < \nu_{\rm c}$ (ISM)	$\frac{p-1}{2}$	$\frac{3(p-1)}{4}$	$\frac{(2p-6)+(p+3)q}{4}$
$\nu_{\rm m} < \nu < \nu_{\rm c}$ (wind)	$\frac{p-1}{2}$	$\frac{3p-1}{4}$	$\frac{(2p-2)+(p+1)q}{4}$
$\nu_{\rm c} < \nu$ (ISM/wind)	$\frac{p}{2}$	$\frac{3p-2}{4}$	$\frac{(2p-4)+(p+2)q}{4}$

Table 4. Mean values and standard deviations for the distribution of the luminosity rest-frame L_R at different times. LZ06 refer to values from Liang & Zhang (2006) and N06 to values from Nardini et al. (2006). See text for more details.

Sample	log L_R (t = 1 day) [erg s^{-1}]	(t = 12 hours) [erg s^{-1} Hz^{-1}]	(t = 10 min) [erg s^{-1}]
LZ06 dim	44.66 ± 0.41	—	—
LZ06 lum	46.15 ± 0.77	—	—
N06	—	30.65 ± 0.28	—
Our result	44.25 ± 0.70	29.54 ± 0.67	46.55 ± 1.23